1-1-2015

Evidence for a Far-Traveled Thrust Sheet in the Greater Himalayan Thrust System, and an Alternative Model to Building the Himalaya

S. Khanal
University of Alabama

D. M. Robinson
University of Alabama

M. J. Kohn
Boise State University

S. Mandal
University of Alabama

AGU PUBLICATIONS

Tectonics

RESEARCH ARTICLE
10.1002/2014TC003616

Key Points:
- The Galchhi shear zone predates the Main Central Thrust
- Similar timing, age, and metamorphism to the intra–Greater Himalayan thrusts
- Kathmandu klippe is the leading edge of an intra–Greater Himalayan thrust

Supporting Information:
- Readme
- Figure S1
- Figure S2
- Text S1
- Table S1

Correspondence to:
S. Khanal,
skhanal@crimson.ua.edu

Citation:
Khanal, S., D. M. Robinson, M. J. Kohn, and S. Mandal (2015), Evidence for a far-traveled thrust sheet in the Greater Himalayan thrust system, and an alternative model to building the Himalaya, *Tectonics*, *34*, 31–52, doi:10.1002/2014TC003616.

Received 17 APR 2014
Accepted 4 DEC 2014
Accepted article online 5 DEC 2014
Published online 15 JAN 2015

Evidence for a far-traveled thrust sheet in the Greater Himalayan thrust system, and an alternative model to building the Himalaya

S. Khanal[1], D. M. Robinson[1], M. J. Kohn[2], and S. Mandal[1]

[1]Department of Geological Sciences, University of Alabama, Tuscaloosa, Alabama, USA, [2]Department of Geosciences, Boise State University, Boise, Idaho, USA

Abstract The Galchhi shear zone underlies the Kathmandu klippe in central Nepal and has emerged as a key structure for discriminating competing models for the formation of the Himalayan orogenic wedge. New chronologic data from the Galchhi area suggest a new structural and orogenic interpretation. Zircons from quartzites and an orthogneiss restrict protolith deposition to between 467 + 7/ − 10 Ma and ~570 Ma, with metamorphic zircon growth at 23–29 Ma. Comparable data from the Greater Himalayan Sequence (GHS) at the intra-GHS Langtang thrust, north of Galchhi, similarly restrict GHS deposition to between 475 + 7/ − 3 and ~660 Ma. Undeformed pegmatites near Galchhi constrain movement of the Galchhi shear zone to ≥22.5 ± 2.3 Ma, long before slip of the Main Central Thrust in the region (≤17 Ma). Shear sense indicators in the Galchhi area indicate both top-to-the-south and top-to-the-north shears. The old age of movement, Neoproterozoic youngest detrital zircons, occurrence of top-to-the-south shear sense indicators, and intrusive Paleozoic granites, all suggest that the Galchhi shear zone is an intra-GHS top-to-the-south thrust, rather than either a thrust involving Lesser Himalayan rocks, or a top-to-the-north shear zone that juxtaposed Tethyan and GHS rocks during coeval movement of the Main Central Thrust. The GHS in Nepal was not emplaced as a single body of rock but consists of at least two ductile "thrust sheets," present in both the hinterland at Langtang and toward the foreland at Galchhi. GHS thrust sheets sequentially underplated during southward propagation of the thrust belt.

1. Introduction

The Himalaya-Tibet orogen is the premier example of an active continent-continent collisional belt (Figure 1) and forms a natural laboratory for testing ideas and validating models regarding mountain building. Recent studies hypothesize that interactions of crustal flow in response to topographic loading and focused erosion on the mountain front control the tectonic evolution of the Himalayan thrust belt [e.g., *Beaumont et al.,* 2001, 2004; *Jamieson et al.,* 2002, 2004; *Grujic,* 2006; *Thiede et al.,* 2004, 2005]. Alternatively, thrust belt evolution may be controlled tectonically by the boundary conditions of a critical wedge [*Davis et al.,* 1983; *Dahlen and Suppe*, 1984], rather than responding directly to climate. In the critical wedge model, the Himalayan thrust belt underplates progressively younger and lower metamorphic grade thrust sheets, and each thrust sheet is kinematically distinct [e.g., *DeCelles et al.,* 2001; *Avouac*, 2003; *Robinson et al.,* 2003, 2006; *Bollinger et al.,* 2006; *Kohn*, 2008; *Herman et al.,* 2010].

Studies in the central Himalaya have focused on the metamorphic core, elucidating the deformation and metamorphic history of the Greater Himalayan Sequence (GHS) [e.g., *Inger and Harris*, 1992; *Macfarlane,* 1993, 1995; *Fraser et al.,* 2000; *Catlos et al.,* 2001; *Kohn et al.,* 2004; *Kohn*, 2008]. Recent research in Nepal suggests that shear zones within the GHS were active 16–27 Ma [*Kohn et al.,* 2004; *Goscombe et al.,* 2006; *Carosi et al.,* 2007, 2010; *Corrie and Kohn*, 2011; *Imayama et al.,* 2012; *Montomoli et al.,* 2013], prior to slip on the Main Central Thrust (10–17 Ma) [*Kohn et al.,* 2004; *Montomoli et al.,* 2013]. In the central Himalayan thrust belt, an isolated klippe of crystalline rocks above the Lesser Himalayan rock, the Kathmandu klippe, is interpreted as an erosional outlier of the Greater and Tethyan Himalayan Sequences [*Stöcklin,* 1980; *Gehrels et al.,* 2006]. Studies of shear zones in the Kathmandu klippe, including the Galchhi shear zone that bounds the klippe [*Rai et al.,* 1998; *Upreti and Le Fort,* 1999], do not specify the timing of activation, which is important for discriminating among structural/tectonic models.

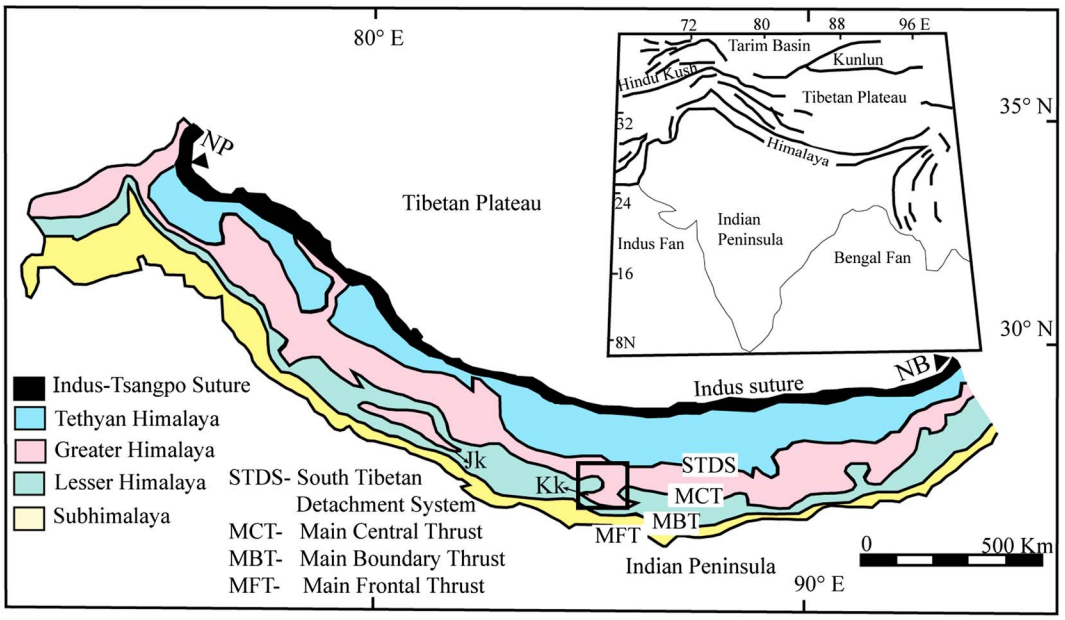

Figure 1. Simplified tectonic map of the Himalayan orogeny showing major lithotectonic divisions (modified from *Paudel and Arita* [2000]). Black box in the Himalaya indicates the study area in Figure 2. Inset shows the Himalayan-Tethyan orogenic system with major faults in bold black. NP: Nanga Parbat; NB: Namche Barwa, Kk: Kathmandu klippe; Jk: Jajarkot klippe.

Several different hypotheses have been proposed for the structural significance of rocks in the Kathmandu klippe and its underlying fault(s), including the (local) Galchhi shear zone on the western side of the klippe. Many correlate the Galchhi shear zone with the Main Central Thrust (MCT), either directly ("1-thrust MCT," juxtaposing GHS and Lesser Himalayan sequence (LHS)) [*Pearson*, 2002; *Gehrels et al.,* 2003, 2006], or as a branch of the MCT but within LHS rocks ("2-thrust, intra-LHS") [*Rai et al.,* 1998; *Upreti*, 1999; *Upreti and Le Fort*, 1999]. *Webb et al.* [2011a] propose a "passive roof thrust" model in which the Galchhi shear zone correlates with the South Tibetan Detachment system (STDS) that juxtaposes Tethyan Himalayan sequence (THS) over GHS and accommodates tens of kilometers of north directed slip. A final model, not previously considered, is that the Galchhi shear zone is the southern continuation of an intraformational thrust within the GHS ("2-thrust, intra-GHS"; this study). To test these proposed models, we examined crosscutting relationships between intrusions and shear fabrics and acquired tectonically discriminating U-Pb ages of zircons and zircon domains from rocks in the Galchhi area and in the core of the GHS farther north at Langtang. Chronologic data include crystallization ages from leucogranite veins that crosscut the Galchhi shear zone, granitic orthogneiss crystallization and metamorphic ages, and detrital ages from quartzites.

2. Orogenic Framework

The Himalaya-Tibet orogen formed when the Tethys oceanic plate subducted northward beneath the Asian plate, and India and Asia collided at ~ 55 Ma along the Indus suture zone (Figure 1) [e.g., *Rowley*, 1996; *Najman et al.,* 2010]. Plate convergence rates changed from ~15 cm/yr at 50 Ma to ~ 4 cm/yr at 35 Ma [*Copley et al.,* 2010], which broadly coincides with the onset of imbrication of the upper crust of the Indian plate [*Powell and Conaghan*, 1973; *Le Fort,* 1975] and deformation in the northern Tibetan part of the fold-thrust belt from the early Eocene to Oligocene time (55–25 Ma) [*Ratschbacher et al.,* 1994; *Zhang and Guo*, 2007]. After ~26 Ma [e.g., *Harrison et al.,* 1992; *Hodges et al.,* 1996; *Coleman*, 1996; *Guillot*, 1999], deformation in Nepal shifted southward, where it was first accommodated by intraformational thrusts/shear zones within GHS, active between 27 and 16 Ma [*Kohn et al.,* 2004; *Goscombe et al.,* 2006; *Carosi et al.,* 2007, 2010; *Corrie and Kohn*, 2011; *Imayama et al.,* 2012; *Montomoli et al.,* 2013]. The deformation locus then migrated farther south, first to the MCT, which was active between 17 and 10 Ma [*Kohn et al.,* 2004; *Montomoli et al.,* 2013], then to faults within the Lesser Himalayan Sequence, such as the Ramgarh-Munsiari thrust and Lesser Himalayan duplex [*Catlos et al.,* 2001; *Robinson et al.,* 2003; *Kohn et al.,* 2004; *Bollinger et al.,* 2006;

Herman et al., 2010; *Khanal and Robinson*, 2013]. Active deformation of Lesser Himalayan rocks ended with the emplacement of the Main Boundary thrust. Finally, Tertiary Subhimalayan rocks were deformed at the frontal part of the thrust belt [*Lavé and Avouac*, 2000] by the Main Frontal thrust, which passively translated, uplifted, and folded the rock in the thrust belt. All thrusts are interpreted to sole into a décollement, the Main Himalayan thrust, which is a gently north dipping shear zone above Indian basement [*Zhao et al.,* 1993].

3. Geology

3.1. Tectonostratigraphy and Structural Geology

Movements on several major thrusts control the structural architecture of central Nepal. From north to south, these structures are South Tibetan Detachment system (STDS) [*Burchfiel et al.,* 1992], Langtang thrust (LT) [*Kohn et al.,* 2004], Main Central Thrust (MCT) [review in *Yin*, 2006], Ramgarh-Munsiari thrust (RMT) [review in *Robinson and Pearson*, 2013], Trishuli thrust (TT) [*Pearson,* 2002; *Khanal and Robinson*, 2013], Lesser Himalayan duplex (LHD) [*DeCelles et al.,* 2001; *Robinson et al.,* 2003, 2006; *Khanal and Robinson*, 2013], Main Boundary thrust (MBT) [*Heim and Gansser*, 1939], and the Main Frontal thrust (MFT) [*Gansser,* 1964; *Lavé and Avouac*, 2000]. From north to south, four fault-bounded lithotectonic zones are recognized [e.g., *Gansser,* 1964; *Le Fort,* 1975]: the Tethyan Himalayan sequence (THS), Greater Himalayan sequence (GHS), Lesser Himalayan sequence (LHS), and Subhimalaya (SH) (Figure 1). A foreland basin system, the Indo-Gangetic plain is present south of the modern Himalaya and formed as a flexural response to crustal thickening [*Lyon-Caen and Molnar*, 1985].

The THS is bounded between the STDS to the south and Indus suture zone to the north (Figure 1), and in the Kathmandu region represents the deformed remnants of a Cambrian to Late Cretaceous passive margin sequence on the northern edge of Greater India [*Brookfield*, 1993; *Colchen et al.,* 1986]. The STDS is a low-angle top-to-the-north brittle-ductile fault system structurally between the GHS and THS, although ductile portions of the STDS arguably deform the uppermost units of the GHS [*Caby et al.,* 1983*; Burchfiel et al.,* 1992; *Carosi et al.,* 1998; *Searle and Godin*, 2003; *Searle*, 2010]. Ductile shear on the STDS, which some propose is genetically linked to movement on the MCT, ended by 19–23 Ma in Nepal [*Hodges et al.,* 1996; *Godin et al.,* 2001; *Searle and Godin*, 2003; *Carosi et al.,* 2013].

The GHS is bounded between the STDS to the north and MCT to the south (Figure 1) and contains Neoproterozoic to Cambrian metasediments intruded by and/or interlayered with orthogneiss interpreted to represent deformed Cambrian-Ordovician granite intrusions [*Parrish and Hodges,* 1996; *DeCelles et al.,* 2000; *Gehrels et al.,* 2003; *Martin et al.,* 2005]. The MCT is a ductile shear zone that juxtaposes high-grade GHS paragneisses and orthogneisses with Paleoproterozoic LHS and is a central component in orogenic models proposed for the tectonic evolution of the Himalayan thrust belt (see summaries of *Hodges* [2000], *Yin and Harrison* [2000], and *Yin* [2006], also more specific models of *Beaumont et al.* [2001], *Robinson et al.* [2003], *Kohn* [2008], and *Webb et al.* [2011a]). Traditionally, initial movement on the MCT was thought to have occurred at 20–22 Ma based on Rb-Sr mica ages, $^{40}Ar/^{39}Ar$ ages from hornblende, biotite and potassium feldspar, and monazite U-Pb ages in garnets from GHS gneiss [*Inger and Harris*, 1992; *Hubbard and Harrison*, 1989; *Harrison et al.,* 1995; *Hodges et al.,* 1996; *Catlos et al.,* 2001; *Godin et al.*, 2001]. However, several complicating factors affect these interpretations, including age interpretation ambiguities [e.g., *Harrison et al.*, 2002; *Kohn et al.*, 2005] and important differences in how studies define and locate the MCT [e.g., *Searle et al.*, 2008; *Kohn*, 2008]. For example, *Kohn et al.* [2005] note that many of the older metamorphic and deformation ages derive from high structural levels in the GHS and probably reflect movement on intra-GHS thrusts, not the MCT in a strict sense. Based on petrogenetically validated, chemically correlated monazite ages, movement of the MCT in central and western Nepal occurred between ~17 and ~10 Ma [*Kohn et al.*, 2004, 2005; *Montomoli et al.*, 2013]. A maximum age of initial movement of circa 20 Ma in central Nepal [*Corrie and Kohn*, 2011] is consistent with these other studies. Intra-GHS thrusts at higher structural levels are older, with movement broadly constrained between ~27 and ~16 Ma [*Kohn et al.*, 2004; *Goscombe et al.*, 2006; *Carosi et al.*, 2007, 2010; *Corrie and Kohn*, 2011; *Imayama et al.*, 2012; *Montomoli et al.*, 2013].

Bounded between the MCT and MBT (Figure 1), the LHS consists of subgreenschist to amphibolite facies rock with an estimated stratigraphic thickness of 10 km [*Upreti*, 1999]. The LHS contains Proterozoic sediments and orthogneiss [*Khanal and Robinson*, 2012a; *Khanal et al.*, 2014] with Indian cratonic affinities

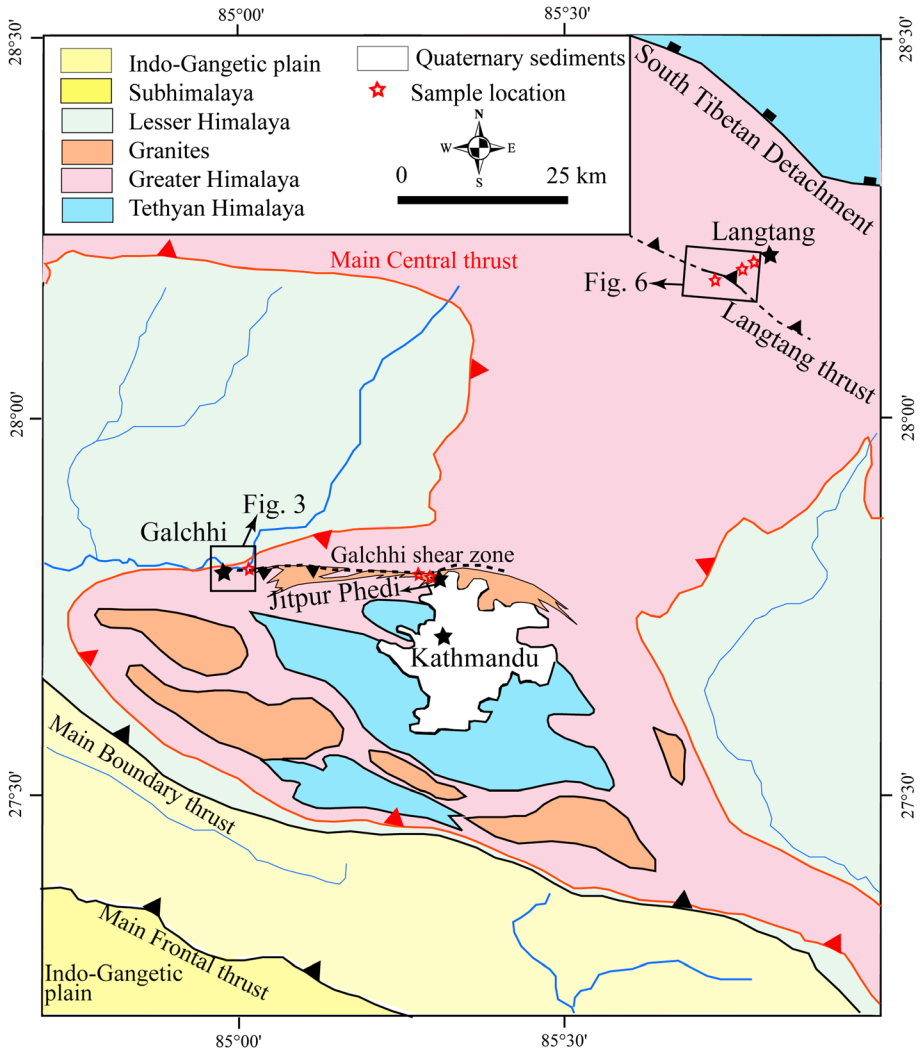

Figure 2. Simplified geological map of the central Nepal Himalaya showing the Kathmandu klippe and associated Cambro-Ordovician granites and Tethyan Himalayan rocks within the klippe. Black star is the location of town or village (modified from *Stöcklin* [1980], *Rai et al.* [1998], *Gehrels et al.* [2006]) MCT = Main Central Thrust; MT = Mahabharat thrust; LT = Langtang thrust; STDS = South Tibetan Detachment system.

that were initially (1.8–1.9 Ga) deposited within a continental volcanic arc setting [*Kohn et al.*, 2010] and succeeded by passive margin sedimentation [*Brookfield*, 1993]. In central Nepal, LHS rocks crop out in a broad E-W trending anticlinorium [*Pêcher*, 1977], which resulted from development of the underlying Lesser Himalayan duplex [*Pearson*, 2002; *Bollinger et al.*, 2004, 2006; *Khanal and Robinson*, 2013]. The RMT is an intra-Lesser Himalayan thrust that emplaces Paleoproterozoic LHS over younger LHS rock and also is a roof thrust of the Lesser Himalayan duplex in western and eastern Nepal [*DeCelles et al.*, 2001; *Robinson et al.*, 2006; *Bhattacharyya and Mitra*, 2009]. The RMT spans the length of the Himalaya and accommodated as much slip as the MCT [see *Robinson and Pearson*, 2013, and references therein]. In central Nepal, in the Langtang and Budhi-Gandaki section, the Trishuli thrust, south of the RMT, is not erosionally breached (it does crop out ~160 km to the west) [*Robinson and Martin*, 2014] and forms the Gorkha-Pokhara antiform [*Pearson*, 2002; *Khanal and Robinson*, 2013]. South of the Trishuli thrust, accretion of the Lesser Himalayan duplex caused southward migration of a ramp along the Main Himalayan thrust [*Khanal and Robinson*, 2013]. Movement of Lesser Himalayan thrust sheets over the ramp in combination with erosion exhumed the Lesser, Greater, and Tethyan Himalayan units [*Khanal and Robinson*, 2013] and tilted and uplifted the MCT, RMT [*Robinson et al.*, 2003], and Trishuli thrust.

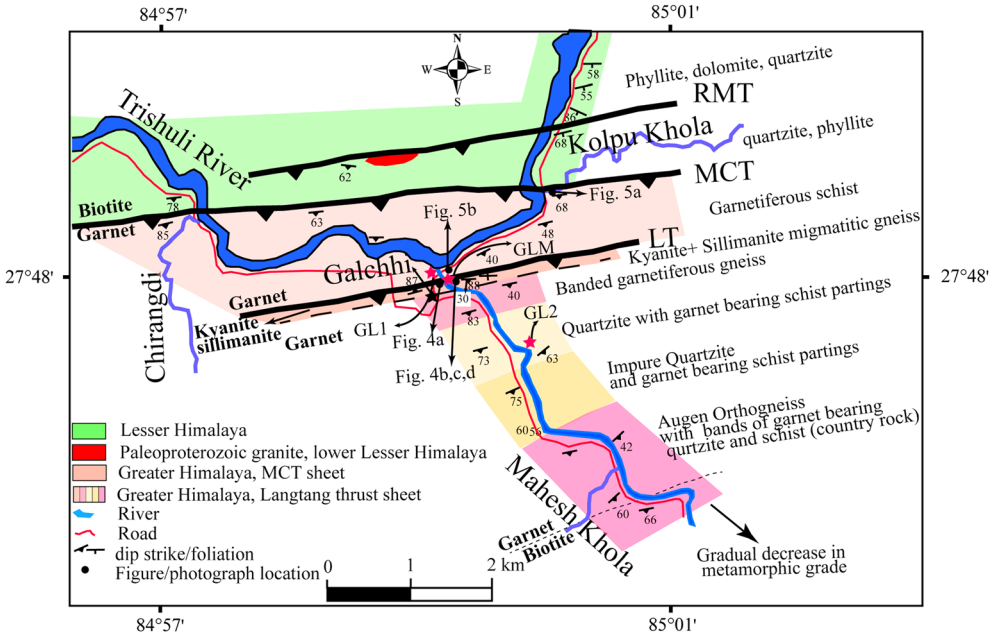

Figure 3. Geological map of Galchhi area with major faults, structural data, and metamorphic isograds, constructed from *Pearson and DeCelles* [2005], *Acharya* [2008], and our own measurements and observations. Figure numbers are labeled on the map. Red star represents the sample location for U-Pb analysis of zircon; black star represent the town of Galchhi; RMT = Ramgarh-Munsiari thrust; MCT = Main Central Thrust; LT = Langtang thrust (Galchhi shear zone). Refer to Figure S1 for Google Earth image of the Galchhi area.

The Subhimalaya is a foreland basin system that incorporated syntectonic sediments during Middle Miocene to Pliocene time (~14–2 Ma) [e.g., *Gautam and Roesler*, 1999; *Ojha et al.*, 2000, 2008]. The Subhimalaya is bounded between the Main Frontal thrust to the south and Main Boundary thrust to the north. The intervening Main Dun thrust repeats Subhimalayan stratigraphy. The Main Frontal thrust is the southernmost boundary of the Himalaya and places the Subhimalayan rocks over modern alluvial sediments.

3.2. Geology of the Kathmandu Klippe and the Galchhi Shear Zone

The Kathmandu klippe (Figure 1) consists of a generally right-way-up sequence with amphibolite facies rocks of the Bhimphedi Group at its base decreasing in metamorphic grade to unmetamorphosed rocks of the Phulchauki Group at its top [*Stöcklin*, 1980]. The Bhimphedi Group consists of garnet- and kyanite-schist, migmatitic gneiss, quartzite, and marble intruded by Cambro-Ordovician granite and Miocene pegmatite [*Johnson et al.*, 2001; *Gehrels et al.*, 2006; *Cawood et al.*, 2007; *Khanal and Robinson*, 2012b]. Neodymium isotopes and occurrence of Cambro-Ordovician granites are similar to GHS rocks exposed elsewhere in Nepal [*Le Fort et al.*, 1986; *Parrish and Hodges*, 1996; *DeCelles et al.*, 2000; *Gehrels et al.*, 2006]. The Lower to Middle Paleozoic Phulchauki Group is correlated with THS rocks to the north based on fossil assemblage and age and consists of calcareous rocks, argillite, and quartz arenite [*Stöcklin*, 1980; *Upreti*, 1999] (Figure 2). *Gehrels et al.* [2006] interpret the THS and GHS contact in the Kathmandu klippe as an angular unconformity based on detrital zircon age populations.

Near Galchhi, at the confluence of the Mahesh Khola and Trishuli River (Figure 3), the base of the Kathmandu klippe is marked by intense shearing, migmatization, and metamorphic and structural discontinuities. Lithologic characteristics include ptygmatic folds of quartz veins (Figure 4a), garnet schist, thin 5–15 cm veins of granitic gneiss alternating with kyanite-garnet schist with late-stage brittle faulting (Figure 4b), sheath folding and boudinage with E-W shearing (Figures 4c and 4d), kyanite- and sillimanite-bearing banded gneiss (Figures 4e and 4f), migmatite, and garnet-bearing quartzite [see also *Webb et al.*, 2011a]. Unusual, elliptical synkinematic garnets occur at Kolphu Khola (Figures 3 and 5a). From north to south (structurally upward), abundances of strain indicators such as quartz ribbons, asymmetric folds, and S-C fabrics first decrease away from the MCT (Figure 5b), then increase toward kyanite-sillimanite-bearing rocks, which contain ptygmatic folds, quartz boudins (Figure 4), and fault striations (Figure 3). These observations indicate two separate shear

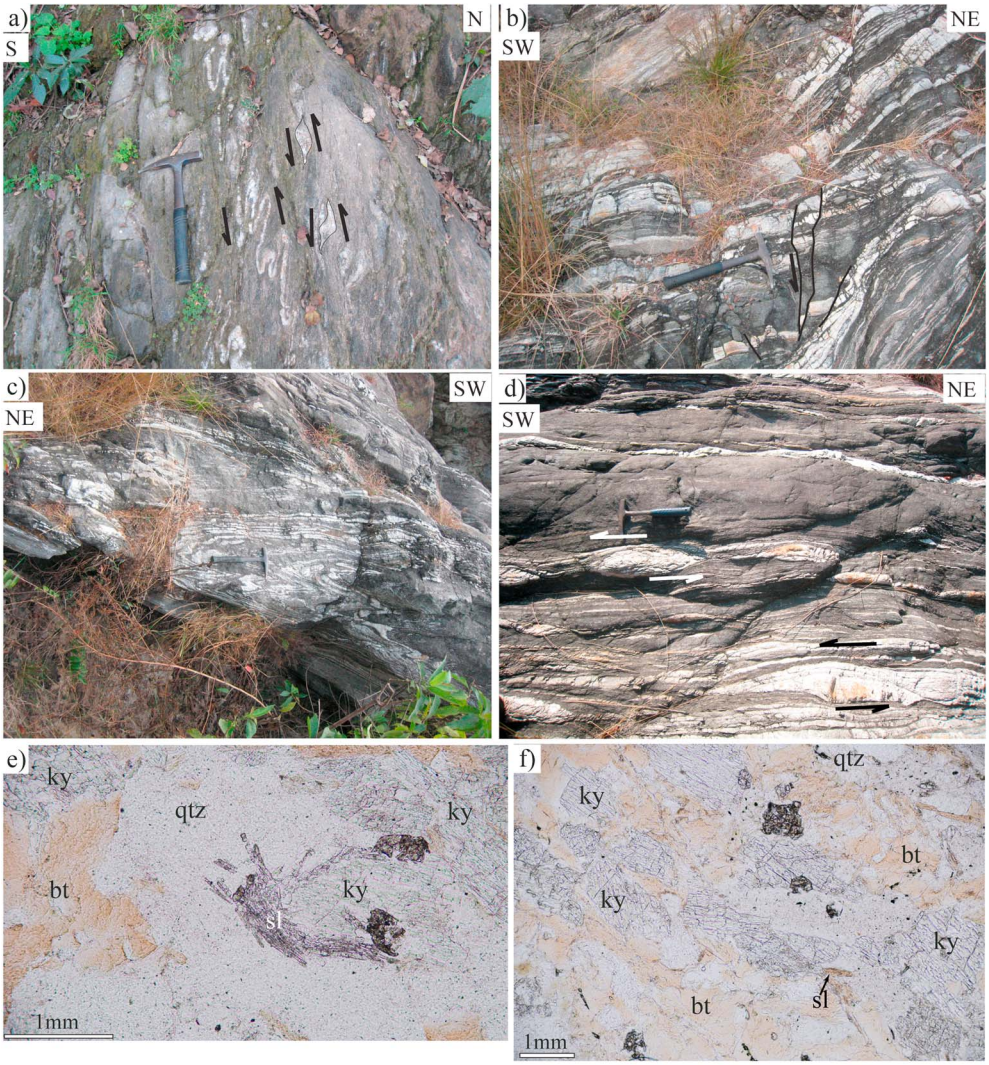

Figure 4. Geology of the Galchhi shear zone. (a) Ptygmatic fold with top-to-the-south sense of shear in the Galchhi shear zone. (b) Five to fifteen centimeters granitic orthogneiss (sample GLM) interbanded with kyanite-garnet-bearing schist with brittle normal faults. (c) Sheath folding with folded orthogneiss and kyanite-garnet-bearing gneiss. (d) Boudinage structure showing E-W sense of shear, 30 cm hammer for scale. (e, f) Photomicrograph of kyanite-sillimanite-bearing gneiss (outcrop shown in Figure 4d) in plane polarized light, parallel to foliation; bt = biotite, qtz = quartz, ky = kyanite, and sl = sillimanite. All photographs are within 20 m of 27.79938°N, 85.48048°E (see Figure 3 for specific locations). S.II and S.III in Figure S1 show additional photographs.

zones, the structurally lower MCT and the structurally higher Galchhi shear zone, also known as the Mahabharat thrust at this location [*Rai et al*., 1998; *Upreti*, 1999; *Webb et al*., 2011a].

Foliations at Galchhi are subvertical and stretching lineations plunge consistently toward the SSW with an average orientation of 30° toward 198. Regionally, rocks dip steeply to the south. The steepness of the foliation is commonly interpreted to result from late-stage folding to form the ESE-WNW trending Kathmandu syncline [*Johnson et al*., 2001; *Gehrels et al*., 2006; *Sapkota and Sanislav*, 2013]. *Webb et al*. [2011a] propose a two-stage unfolding scheme, first rotating rocks ~80° around an approximately E-W trending axis (counterclockwise looking east). This stage restores nearly vertical rocks to a quasi-horizontal orientation. The sense and magnitude of rotation are inescapable because stratigraphically and structurally higher rocks occur to the south and southeast in the core of the Kathmandu klippe. Thus, restoring the Kathmandu klippe's tectonostratigraphy to its prefolding orientation requires a counterclockwise rotation (looking east) in the Galchhi area. This rotation maintains the SSW trend of lineations, and top-to-the-south

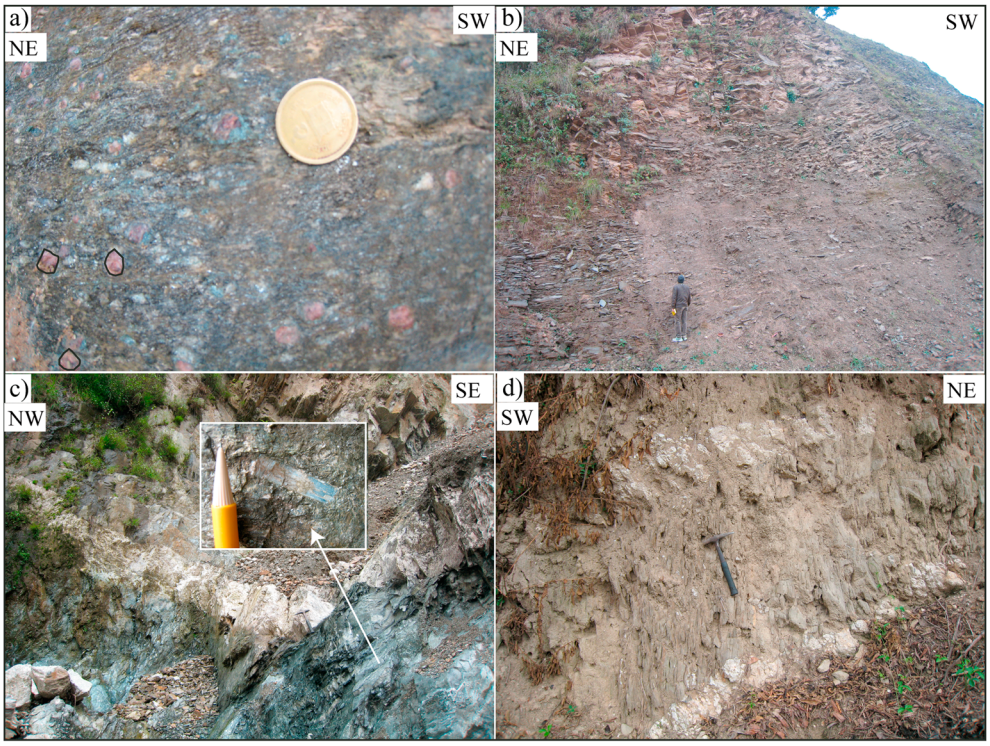

Figure 5. Geology of the Galchhi area (a) Garnetiferous schist near the MCT on the bank of the Kholpu Khola, Rs 2 coin for scale. (b) Impure micaceous quartzite/schist showing decrease in metamorphic grade from the MCT mylonitic zone (Figure 5a) toward south and 200 m north of the Galchhi shear zone (Figure 4), person for scale. (c) Undeformed pegmatite crosscutting kyanite-bearing schist, 30 cm hammer for scale. Inset shows detail of kyanite. (d) Undeformed pegmatite veins cross cutting foliations, 30 cm hammer for scale. Location of the photograph is shown in Figure 3.

(or top-to-the-north) shear senses [see *Webb et al*., 2011a]. *Webb et al*. [2011a] propose a secondary counterclockwise rotation (looking down) to restore stretching lineations to a more N-S orientation. This latter rotation does not affect tectonic interpretations—basically any reasonable restoration of orientations in the context of the overall stratigraphy and structure of the Kathmandu klippe results in a shallow dip with a transport direction oriented between N-S and NE-SW.

Metamorphic grade increases structurally upward from the footwall of the MCT (subgarnet grade) to the hanging wall of the Galchhi shear zone (kyanite/sillimanite gneisses) [*Johnson et al*., 2001]. This metamorphic inversion through the MCT is well documented throughout the Nepal Himalaya [e.g., *Le Fort*, 1975]. Ultimately, metamorphic grade must decrease farther upward because chlorite-grade rocks crop out ~8 km to the south of the Galchhi shear zone [*Johnson et al*., 2001]. However, because rock compositions change so dramatically across strike at the Galchhi shear zone, kyanite- and sillimanite-absent mineral assemblages in hanging wall rocks 0.5–5 km south of the Galchhi shear zone do not necessarily reflect lower metamorphic conditions [*Johnson et al*., 2001]. For example, biotite orthogneiss and garnet quartzite and schist similar to rocks at Galchhi are common in high-grade GHS exposures throughout the Himalaya. Thus, metamorphic parageneses do not demand thinning or flattening, at least in the immediate hanging wall of the shear zone. Although the "isograds" of *Johnson et al*. [2001] accurately depict mineral assemblages (e.g., there is no kyanite south of the "kyanite isograd"), they do not convey temperature information.

Sheared leucocratic segregations in hanging wall migmatites of the Galchhi shear zone have yielded zircon U-Pb crystallization ages of 18 ± 2 Ma [*Johnson et al*., 2001] and 20–30 Ma [*Webb et al*., 2011a]. At Jitpur Phedi, along the northeast extension of the Galchhi shear zone north of Kathmandu, undeformed pegmatite veins crosscut kyanite gneiss (Figure 5c) and schist (Figure 5d).

3.3. Geology of the Langtang Area

The Langtang and Bhotekoshi River valleys expose GHS and LHS units, as well as the Langtang thrust, MCT, and RMT (Figure 6). The intra-LHS RMT carries Paleoproterozoic orthogneiss, garnetiferous schist, and

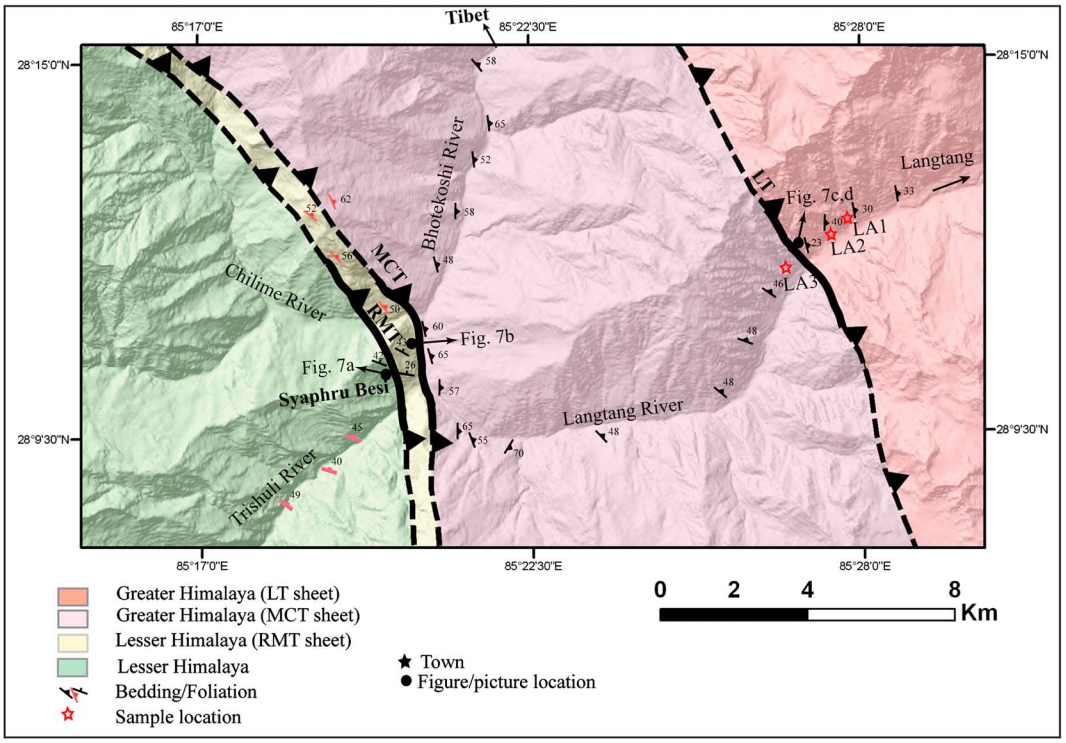

Figure 6. Geologic map of the Syaphru Besi-Langtang area draped over a digital elevation model. All geological data in black are from this study, and red are from *Pearson and DeCelles* [2005]. Figure numbers are labeled on the map. LT = Langtang thrust; MCT = Main Central Thrust; and RMT = Ramgarh-Munsiari thrust.

quartzite over Mesoproterozoic limestone and phyllite (Figures 6 and 7a). We locate the MCT by integrating the $\varepsilon Nd(0)$ data [*Pearson*, 2002] and our own observations of ductile shearing and migmatite. The MCT hanging wall rocks are garnetiferous schist and kyanite-sillimanite-bearing gneiss, migmatitic gneiss with segregated leucosomes, and gneissic intrusions. *Kohn et al.* [2004] hypothesized an intra-GHS thrust, the Langtang thrust (Figure 6), based on differences in pressure-temperature (P-T) conditions, chemical zoning in garnet and monazite, and in situ ^{232}Th-^{208}Pb ages of chemically fingerprinted monazite domains. The Langtang thrust shear zone consists of deformed schist (Figure 7c) with abundant ptygmatic folds, quartz ribbons and microfolds, and with migmatite and sillimanite-K-feldspar grade rocks in the hanging wall (Figure 7d).

4. Models for the Origin of the Kathmandu Klippe

Three different models have been proposed previously for the origin of the Kathmandu klippe, and a new model is proposed here. Each of the four models makes different predictions (Table 1) regarding lithologic affinities of rock in the hanging wall and footwall of the Galchhi shear zone, the sense of shear, and timing of movement of the Galchhi shear zone relative to the MCT.

In the first model (2-thrust, intra-LHS) [*Rai et al.*, 1998; *Upreti and Le Fort*, 1999] the Galchhi shear zone is the top-to-the south Mahabharat thrust with crystalline LHS in its hanging wall and footwall (Figure 8a). The Mahabharat thrust/Galchhi shear zone floors the Kathmandu klippe and predates movement on the structurally higher, out-of-sequence MCT (Figure 8a, model 1), whose nearest exposure occurs north of Kathmandu, ~25 km north (Figure 2).

In the second model (1-thrust, MCT; Figure 8b), the Galchhi shear zone is considered the southern extension of the MCT [*Pandey et al.*, 1995; *Johnson et al.*, 2001; *Gehrels et al.*, 2003]. The hanging wall is GHS, and the local footwall could be either LHS or GHS depending on how the boundaries of the MCT shear zone are defined. Movement is synchronous with the MCT, with top-to-the-south shear sense.

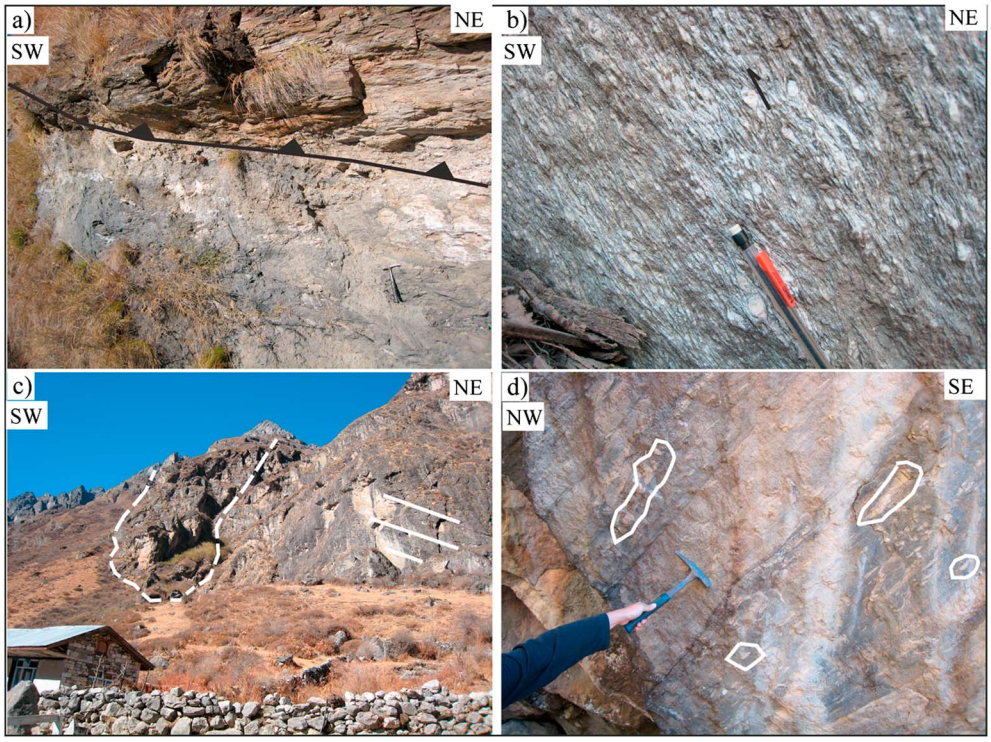

Figure 7. Geology of the Langtang area. (a) The Ramgarh-Munsiari thrust with incompetent phyllitic beds deformed by the overlying Paleoproterozoic quartzite and phyllite, 30 cm hammer for scale. (b) Mylonitic foliation near the MCT showing top-to-the-south sense of shear in LH augen orthogneiss, 15 cm pen for scale. (c) Langtang thrust containing highly deformed schist (dashed white line) with lineations (white lines), abundant ptygmatic folds, microfolds, and quartz ribbons. House for scale. (d) Leucogranite in the hanging wall of the Langtang thrust sheet with a few leucosomes outlined in white; 30 cm hammer for scale. Figure locations are shown in Figure 6. S.IV–S.VI in Figure S1 show additional photographs.

In the third model (passive roof thrust, Figure 8c) [*Webb et al*., 2011a] a wedge of GHS is inserted between THS and LHS rocks. This model correlates the Galchhi shear zone with the STDS, which then represents a back thrust that accommodated tens of kilometers of slip and that merges with the MCT underneath the Kathmandu klippe. Rocks above the Galchhi shear zone have THS affinity, movement is coeval with the MCT, and rocks exhibit top-to-the-north shear sense.

Reconsideration of regional data inspired a new fourth model (Figure 8d) in which the Galchhi shear zone overlies the MCT (in a strict sense) and is the southern continuation of an older intra-GHS thrust, such as the Langtang thrust. The hanging wall rock is GHS and has top-to-the-south sense of shear. To test these models, we investigated fabrics and zircon age systematics of rocks from the hanging wall and footwall of the Galchhi shear zone and Langtang thrust to determine lithologic affinities, shear senses, and ages of movement.

5. Zircon U/Pb Isotopic Dating Methods

We collected three 1–2 kg samples from the hanging wall and footwall of the Langtang thrust near Langtang (Figure 6, locations are given in Table 2). Sample LA2 is an augen orthogneiss, and samples LA1 and LA3

Table 1. Models and Observations for the Formation of the Galchhi Shear Zone

Model		Hanging Wall	Footwall	Sense of Shear	Timing Relative to MCT
1	2-thrust, intra-LHS	LHS	LHS	Top-to-the-south	Predates
2	1-thrust, MCT	GHS	LHS (?)	Top-to-the-south	Coeval
3	Passive roof thrust	THS	GHS	Top-to-the-north	Coeval
4	2-thrust, intra-GHS	GHS	GHS	Top-to-the-south	Predates
Observations		GHS (THS?)	GHS (THS?)	Top-to-the-south, Top-to-the-north	Predates

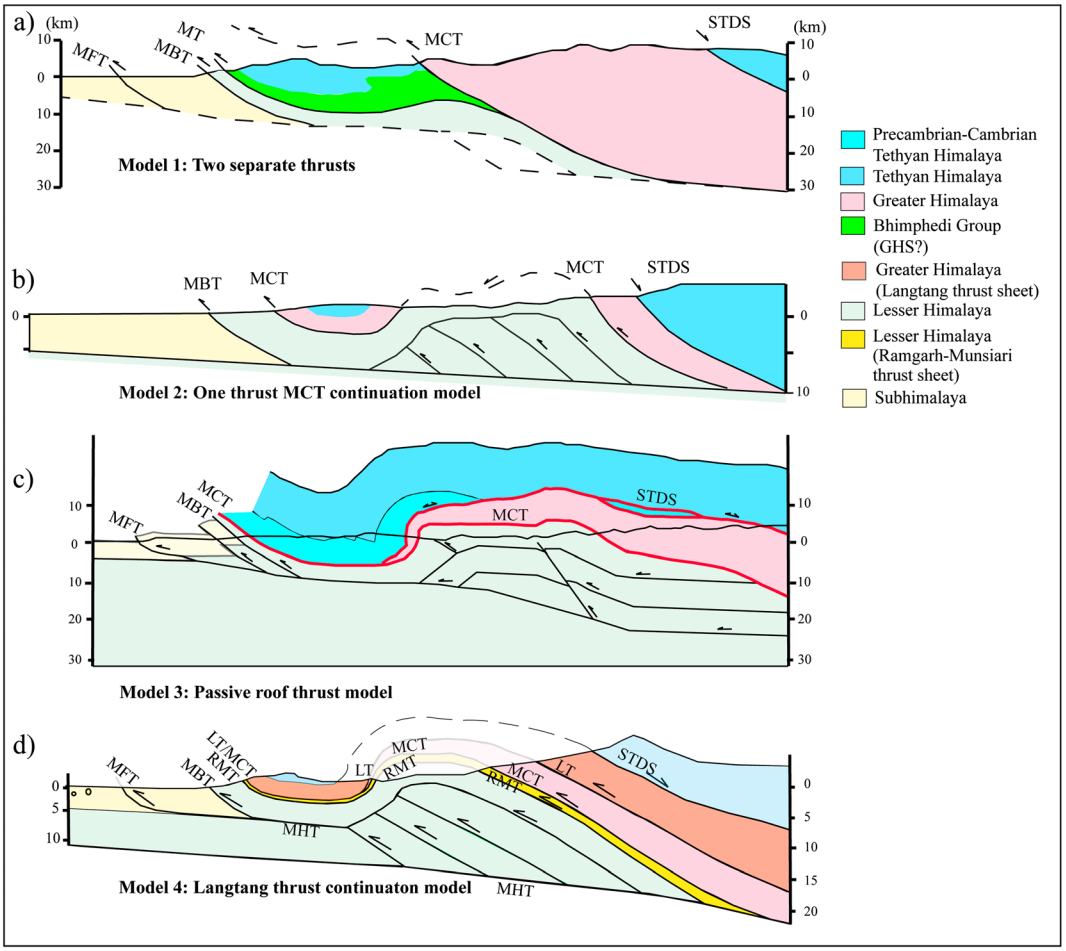

Figure 8. Cross section with different interpretations for the origin of the Kathmandu klippe. (a) Model 1: 2-thrust, intra-LHS. Redrawn from *Upreti and Le Fort* [1999]. (b) Model 2: 1-thrust MCT. Redrawn from *Gehrels et al.* [2003]. Lesser Himalayan duplex structure adopted from *Khanal and Robinson* [2013]. (c) Model 3: passive roof thrust. Redrawn from *Webb et al.* [2011a]. (d) Model 4: intra-GHS thrust. Our interpretation for the origin of the Kathmandu klippe. MCT = Main Central Thrust; MT = Mahabharat thrust; MBT = Main Boundary thrust; MFT = Main Frontal thrust; LT = Langtang thrust; STDS = South Tibetan Detachment thrust.

are micaceous quartzites. We also collected three samples from the hanging wall and footwall of the Galchhi shear zone (Figure 3, locations are given in Table 2). Sample GLM is from a 10 cm thick granitic gneiss, parallel to the foliation of the garnet-kyanite-bearing paragneiss (see Figure S1 in the supporting information). Sample GL1 is an impure micaceous quartzite and sample GL2 is a greenish gray-white quartzite. Samples BL1 and BL2 are undeformed pegmatite veins crosscutting kyanite-bearing gneiss (Figures 5c and 5d) near Jitpur Phedi (Figure 2). Sample processing and analytical methods followed standard practices—see the supporting information for details.

6. Zircon U/Pb Isotopic Dating Results

6.1. Galchhi Shear Zone

Sample GL1 yielded 94 usable dates that reveal major detrital zircon age populations at ~550–750 Ma and 900–1200 Ma, with pronounced peaks at ~632 and ~984 Ma. Older ages (1700–3200 Ma) scatter with no major peaks or pattern. Three grains define the youngest peak at 570 Ma (Figure 9a). Sample GL2 yielded 87 usable dates that reveal major detrital zircon populations at ~550–825 Ma and 850–1200 Ma, with pronounced peaks at ~632 and ~994 Ma. Older ages (1700–3000 Ma) scatter with no major peaks. Four grains define the youngest peak at 584 Ma (Figure 9b). Thus, the maximum depositional ages of the sedimentary

Table 2. Sample Locations and Lithologic Description

Sample	°N (dd.ddddd)	°E (dd.ddddd)	Rock Unit	Description
LA1 Detrital	28.20973	85.48048	Langtang thrust sheet	Garnet-bearing banded gneiss with ptygmatic folds and leucosome
LA2	28.19643	85.45254	Langtang thrust sheet	Augen orthogneiss
LA3 Detrital	28.19544	85.45027	Main Central Thrust sheet in Langtang	Psammitic schist with garnetifierous banded gneiss, abundant quartz segregations
GLM	27.79938	85.00122	Galchhi thrust sheet	Augen orthogneiss (3–10 cm) interband with kyanite-sillimanite-bearing garnetiferous dark schist
GL1 Detrital	27.79997	85.00009	Main Central Thrust sheet in Galchhi	Psammatic schist with thin band of garnetiferous pelitic schist
GL2 Detrital	27.79483	85.00865	Galchhi thrust sheet	White to greenish gray quartzite with bands of garnet-bearing schist
BL1	27.77888	85.28320	NE extent of Galchhi thrust sheet	Undeformed pegmatite vein crosscutting kyanite-bearing schist
BL2	27.78708	85.27353	NE extent of Galchhi thrust sheet	Undeformed pegmatite vein crosscutting foliations of dark schist

protoliths of the metamorphic rock in Galchhi are ~570 Ma for sample GL1 and ~584 Ma for sample GL2. Zircons older than 1400 Ma from both samples GL1 and GL2 are slightly discordant (see Figure S2 in the supporting information).

Igneous zircons from sample GLM are internally heterogeneous with inherited zircon cores, oscillatory zoned magmatic overgrowths, and homogeneous rims (see Figure S2 in the supporting information). Zircon core ages range from 800 to 2600 Ma with age peaks at ~1000 Ma, ~1800 Ma, and one grain at ~2600 Ma. Zircon cores have low to moderate U concentrations (100–700 ppm), and low U/Th ratios of 1–6 (see Figure S2 in the supporting information). Zircons from 800 to 1800 Ma are concordant while the older 2600 Ma zircon is discordant (see Figure S2 in the supporting information). Zircon overgrowths exhibit oscillatory zoning, and ages are concordant, ranging from ~440 to ~515 Ma, including the upper and lower limit of uncertainties (Figure 9c). Because of the scattered ages, probability of the rim average is almost 0. Thus, we used the zircon age extractor algorithm from the Isoplot program [*Ludwig*, 2008] to infer an Early Ordovician ($467 + 7/-10$ Ma, 2σ) crystallization age of the rock protolith (Figure 9d). Zircons of this age contain low to high U concentration (136–3155 ppm), and low U-Th ratio (<5) except four zircons that have a range of ratios from 12 to 23 and that were excluded from the age calculation (Figure 9d) (see Figure S2 in the supporting information for U/Th plot). The homogeneous rims of the zircons are all concordant (Figure 9e) with ages of 23–29 Ma and a weighted mean age of 26.2 ± 1.7 Ma (2σ; Figure 9f). These zircons contain high U concentration (1600–9400 ppm) and a high U-Th ratio (42–2350; see Figure S2 in the supporting information).

6.2. Undeformed Pegmatite Veins

Samples BL1 and BL2 are from undeformed pegmatitic veins crosscutting kyanite-bearing biotite schist along the NE extension of the Galchhi shear zone (Figures 5c and 5d). Zircon grains have extensive radiation damage, and CL images reveal very few zircons suitable for dating. Thin rims surrounding the damaged core of the grains are clearer in CL images (see Figure S2 in the supporting information) and were targeted for analysis.

For sample BL1, ablation of the rim with a 15 μm beam size provided six usable dates that are all concordant (Figure 10a) and range from 20 to 28 Ma. All six analyses yield a weighted mean age of 22.5 ± 2.3 Ma (2σ; Figure 10b), which is not significantly different from the youngest three analyses (circa 21 Ma). We view this age as our best estimate of the timing of melt crystallization.

Sample BL2 also yielded six concordant ages, but these range from ~25 to ~180 Ma (Figure 10c). Younger zircons (~25 Ma) have higher U/Th ratios (38–75) compared to older grains (ratio of 7–35; 84–166 Ma; see Figure S2 in the supporting information). The two youngest ages imply a weighted average age of 24.7 ± 0.6 Ma (2σ) (Figure 10d). The older ages of 84–166 Ma probably represent mixed core-rim ages and are not discussed further. Because of the scatter in concordant ages and the possibility of slight mixing between chronologically distinct domains, we view the ~25 Ma age from BL2 as a maximum for the true age of melt crystallization, rather than a crystallization age in a strict sense.

6.3. Langtang Area

Sample LA1 yielded 80 usable dates with age population peaks at 600–1000 Ma and 1500–1900 Ma and scattered older ages from 2200 to 2800 Ma (Figure 11a). Probability maxima occur at ~825 Ma (20 grains), and

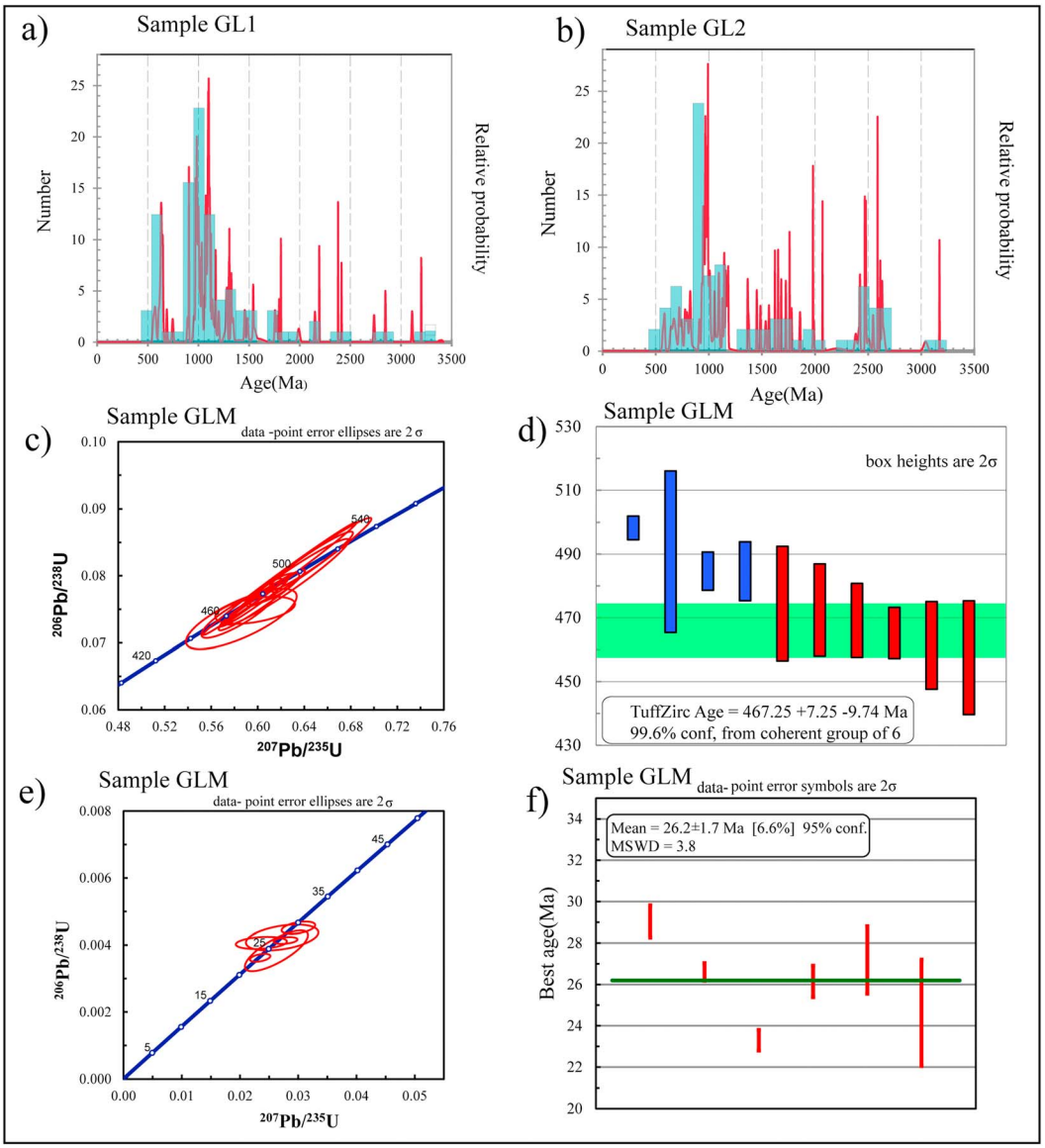

Figure 9. U/Pb zircon analysis of samples from Galchhi area. (a, b) Relative probability plots (red lines) and histogram (blue rectangles) for detrital zircon ages from sample GL1 and GL2 from Galchhi, respectively. (c) U/Pb concordia diagrams for zircons from augen orthogenesis sample GLM. (d) Crystallization age of the augen orthogneiss inferred using the zircon age extractor function of Isoplot [*Ludwig*, 2008]. (e) U/Pb concordia diagram of zircon rims from sample GLM. (f) Weighted mean age of zircon rims. Sample locations shown in Figure 3.

at ~1600 Ma, ~1710 Ma, and ~2500 Ma. Twelve grains define the youngest peak at 765 Ma. Sample LA3 yields 89 usable dates that cluster into three distinct age groups at circa 600–1000 Ma, 1500–1700 Ma, and 2300–2600 2Ma (Figure 11b). Probability maxima occur at ~843 Ma (40 grains), ~1628 Ma (10 grains), and ~2471 Ma (12 grains). Four grains define the youngest peak at ~660 Ma (see Figure S2 in the supporting information for concordia plot).

Zircons from sample LA2 are prismatic, and a few zircons contain rounded to subrounded inherited cores surrounded by mainly oscillatory zoned magmatic overgrowths (see Figure S2 in the supporting information). All analyses are concordant (Figure 11c). Oscillatory zoned regions in 17 grains have crystallization ages that range from 440 to 532 Ma (Figure 11d). The zircon age extractor algorithm from Isoplot [*Ludwig*, 2008] implies an earliest Ordovician ($475 + 7/-3$ Ma, 2σ) crystallization age of the protolith. Eight ages of zircon cores range from 600 to 1275 Ma (see Figure S2 in the supporting information).

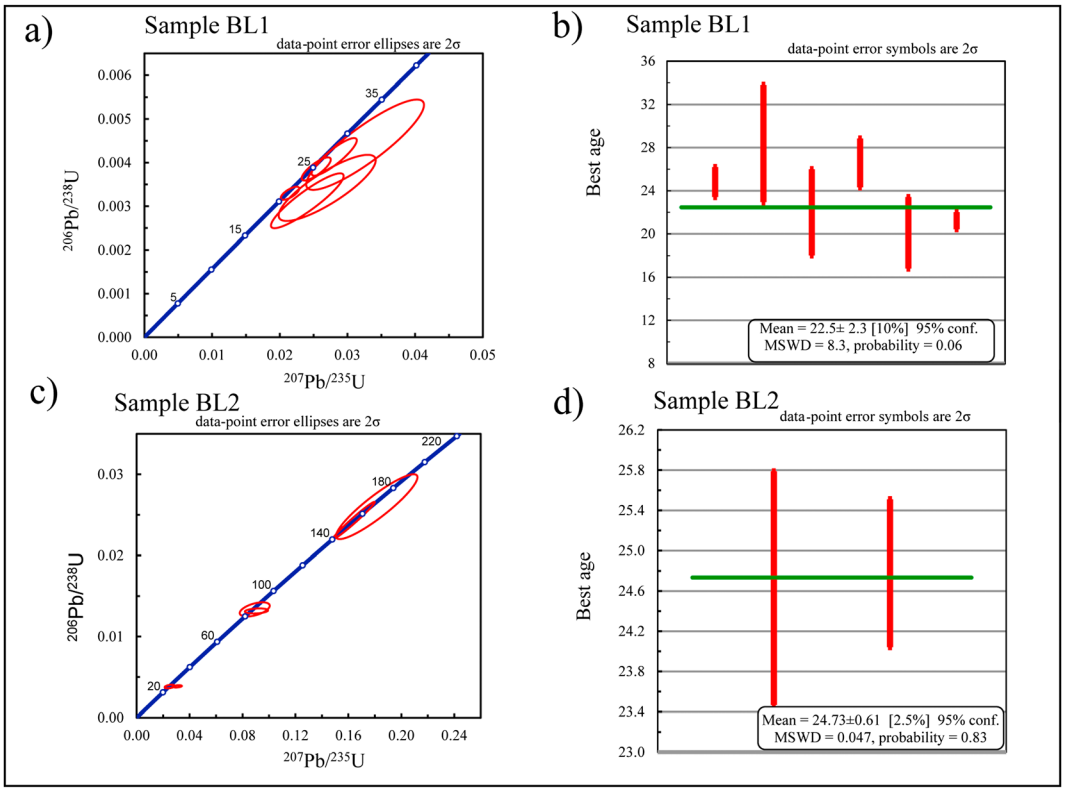

Figure 10. U/Pb zircon analysis from pegmatites. (a) U/Pb concordia diagram of zircons analyzed from undeformed pegmatite sample BL1. (b) Weighted average of zircon ages. (c) U/Pb concordia diagram of zircons analyzed from undeformed pegmatite sample BL2. (d) Weighted average of the youngest two grains. MSWDs: mean square weighted deviates. Sample locations shown in Figure 2.

7. Interpretations

7.1. Galchhi and Surrounding Area

In sample GLM, the 23–29 Ma zircon rims have high U/Th ratios (40–1200) compared to the magmatic portion of the zircons analyzed from the same sample with 440–515 Ma ages (U/Th = 1–24; see Figure S2 in the supporting information). High U-Th ratios are consistent with metamorphic growth [*Rubatto*, 2002], and because zircon solubility decreases during cooling [*Watson and Harrison*, 1983], these hanging wall ages may reflect zircon growth during cooling associated with shear zone activity at that time. Alternatively, if zircon rims recrystallized during prograde metamorphism, these ages bound the maximum possible initiation of the Galchhi shear zone (≤ ~ 23 Ma). The rim ages from the undeformed pegmatite zircons (BL1 and BL2) of ≤ ~25 Ma and 22.5 ± 2.3 Ma limit the youngest possible movement of the NE extent of the Galchhi shear zone. Thus, shear zone activity is broadly limited between 29 and 20 Ma (if GLM zircon rims reflect cooling during shearing), and possibly limited to a brief pulse at ~23 Ma (if GLM zircon rims are prograde and predate shearing).

Samples GL1 and GL2 from the hanging wall of the Galchhi shear zone (Figure 3) have the youngest detrital zircon age peaks at ~570 Ma and ~584 Ma (Figure 9). The abundance of Neoproterozoic zircons rules out correlation to the lower Paleoproterozoic LHS. Rather, age spectra are most similar to Neoproterozoic GHS [*Martin et al*., 2005; *Gehrels et al*., 2011] with broad peaks at ~630, 1000, and 1100 Ma. Correlation seems less likely with THS rocks, which show broad peaks at 1050 Ma and ~530 Ma [*Myrow et al*., 2003, 2009; *DeCelles et al*., 2004] and may contain detrital zircons as young as 460 Ma [*Gehrels et al*., 2003]. Whereas Neoproterozoic THS rocks do occur elsewhere in the Himalaya (e.g., NW India) [*Webb et al*., 2011b], evidence for correlative units (the Sanctuary Formation) in this region of Nepal is otherwise lacking [*Stöcklin*, 1980; *Gehrels et al*., 2003]. Overlapping ages of interspersed Ordovician granites between Galchhi and Langtang, and the general lack of granites in THS rocks regionally, further support a GHS correlation. Thus, we favor a GHS protolith for both levels, although the depositional age of these rocks is most conservatively bracketed

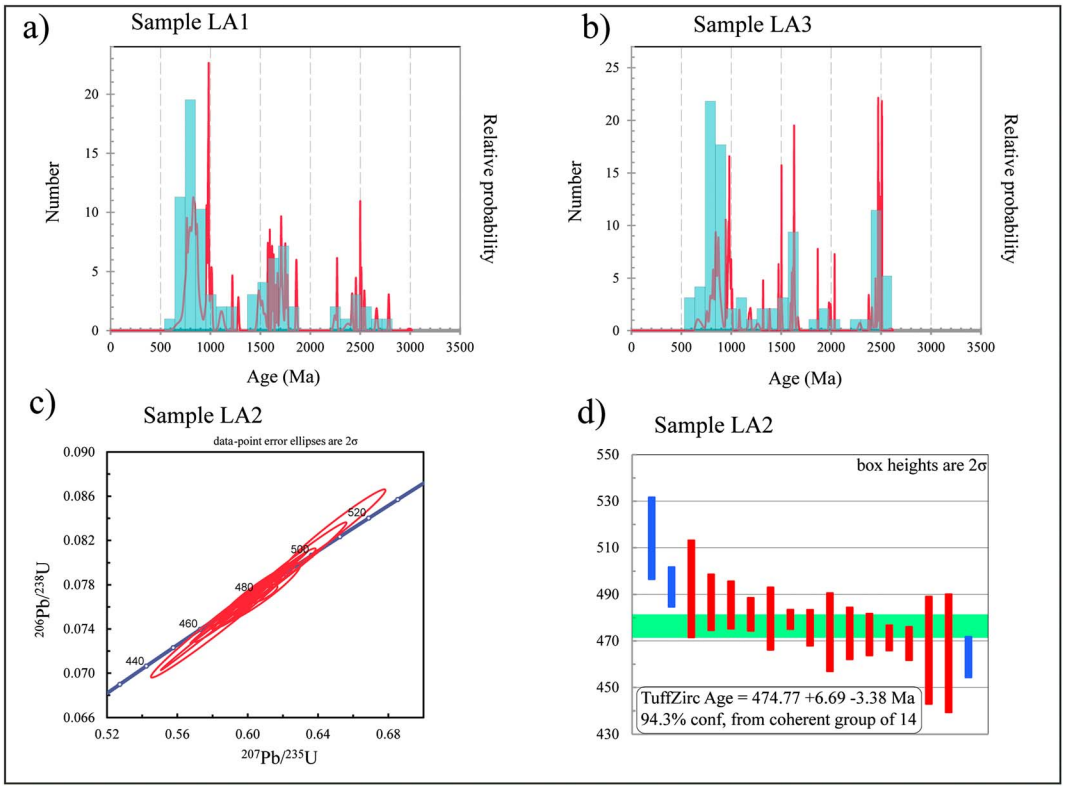

Figure 11. U/Pb zircon analysis from Langtang area. (a, b) Relative probability plots (red lines) and histogram (blue rectangles) for detrital zircon ages from sample LA1 and LA3, respectively. (c) U/Pb concordia diagrams for augen orthogenesis (LA2) zircons. (d) Crystallization age of the augen orthogneiss inferred using the zircon age extractor function of Isoplot [*Ludwig,* 2008]. Sample locations shown in Figure 6.

only between ~570/~580 Ma (youngest detrital zircons) and ~470 Ma (intrusion age of granites) so that the hanging wall and footwall of the Galchhi shear zone could in principle be either GHS or THS.

7.2. Langtang Area

Samples of micaceous quartzite from the GHS in the Langtang thrust footwall (LA3) and hanging wall (LA1) show no ages younger than ~660 Ma (LA3) and ~765 Ma (LA1), and age spectra show broad peaks at ~800 and 1000 Ma. Together with a crystallization age of 475 + 7/ − 3 for orthogneiss sample LA2, these data bracket the age of the GHS protolith in Langtang to between ~660/765 Ma and ~475 Ma. Like GL1 and GL2 from Galchhi, poor correlation of age spectra with Paleozoic rocks tends to favor a Neoproterozoic depositional age; although a Paleozoic age is possible.

8. Discussion

The early history of the India-Asia collision, from ~55 Ma to ~20 Ma, is poorly known. As discussed previously, studies that link accessory mineral chemistry and ages with metamorphic parageneses suggest an age of 16–17 Ma for the initiation of MCT movement in central Nepal [*Kohn et al.*, 2004, 2005; *Montomoli et al.*, 2013]. The MCT is commonly assumed to be the first major thrust south of the THS [e.g., *Hubbard and Harrison*, 1989; *Inger and Harris*, 1992; *Hodges et al.*, 1996; *Harrison et al.*, 1997; *Arita et al.*, 1997; *Johnson and Rogers*, 1997; *Coleman*, 1998; *Catlos et al.*, 2001; *Johnson et al.*, 2001; *Webb et al.*, 2011a]. However, a growing body of evidence indicates that structurally higher, intra-GHS thrusts were active between 16 and 27 Ma and thus predate slip on the MCT. These thrusts include the Langtang, Sinuwa, and Bhanuwa thrusts in central Nepal [*Kohn et al.*, 2004; *Martin et al.*, 2010; *Corrie and Kohn*, 2011], the Toijem and Magri shear zones in western Nepal [*Carosi et al.*, 2007, 2010; *Iaccarino et al.*, 2012, 2013; *Montomoli et al.*, 2013], and the High Himalaya thrust in far eastern Nepal [*Imayama et al.*, 2012]. Some studies advocate out-of-sequence thrusting at a local scale in the GHS in central Nepal [*Parrish and Hodges*, 1996; *Wobus et al.*, 2003, 2006; *Huntington et al.*, 2006] and Bhagirathi River, India

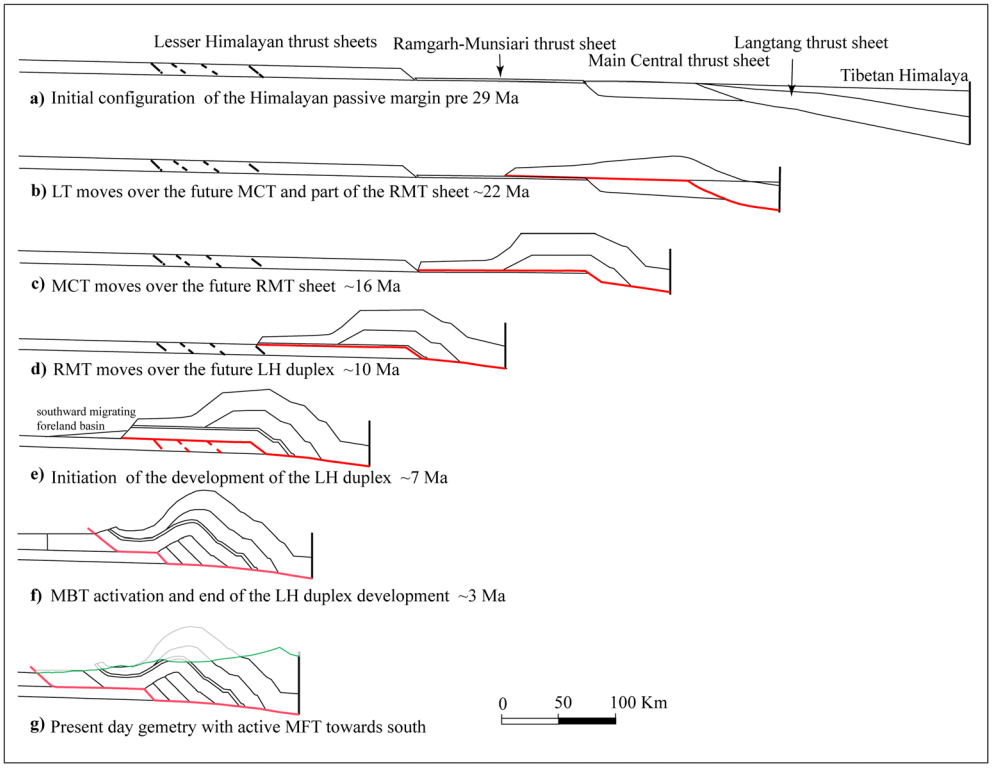

Figure 12. (a–g) Kinematic sequence of deformation of the Langtang-Galchhi section central Nepal. Each thrust sheet is defined in the initial configuration. Red line indicates the active fault. Green color represents present-day erosional surface, and the translucent region represents eroded material. Timing of each fault is defined in text. LT = Langtang thrust; MCT = Main Central Thrust; RMT = Ramgarh-Munsiari thrust; LH = Lesser Himalaya; MFT = Main Frontal thrust.

[*Mukherjee*, 2013]. However, the location, precise timing, and magnitudes of these out-of-sequence thrust events are poorly known and may represent location-specific unique complications, for example, relatively minor adjustments to tilting and folding on underlying structures.

Lithologically, we cannot always discriminate GHS from THS rocks, but the lack of LHS rocks in the hanging wall or footwall of the Galchhi shear zone and the map/structural data rules out model 1 (2-thrust, intra-LHS thrust model). Otherwise, the somewhat greater likelihood that rocks belong to the GHS tends to support model 4 (2-thrust, intra-GHS) but does not uniquely exclude models 2 (1-thrust MCT) or 3 (passive roof thrust).

Microstructurally and mesostructurally, *Webb et al.* [2011a] emphasize the occurrence of top-to-the-north shear at high temperature at the Galchhi shear zone in support of the passive roof thrust model, which is the only model that requires top-to-the-north shear (model 3, Table 1). Top-to-the-north shear sense indicators do occur in the Galchhi shear zone, but so do top-to-the-south shear sense indicators (e.g., Figure 4d). Indeed, a comprehensive study of shear indicators around the Galchhi shear zone [*Sapkota and Sanislav*, 2013] revealed both top-to-the-south and top-to-the-north indicators for the earliest generations of synmetamorphic and early postmetamorphic structures. Thus, although some shear sense indicators are consistent with model 3, they are also consistent with all models.

Overall, chronologic constraints are most diagnostic: the timing of movement of the Galchhi shear zone is constrained between 20 and 29 Ma, *prior* to movement on the MCT in this sector. Excluding model 1 on stratigraphic grounds, this observation uniquely supports model 4 and the view that the Galchhi shear zone represents an older intra-GHS thrust such as the Langtang, Sinuwa, or Bhanuwa thrusts. This interpretation is consistent with previously published data from deformed leucocratic segregations at Galchhi. *Johnson et al.* [2001] infer the latest stages of deformation as occurring by 18 ± 2 Ma (although they also report a maximum age of 21 Ma), and *Webb et al.* [2011a] prefer an age of deformation sometime after 24–30 Ma. Although these ages might possibly be reconciled with movement coeval with the MCT (models 2 and 3), they are also consistent with model 4.

Published chronologic data in the region further support an older origin of the Galchhi shear zone. *Arita et al*. [1997] present a $^{40}Ar/^{39}Ar$ age of 14–15 Ma close to the MCT north of the Kathmandu klippe along the Trishuli-Hetaunda section and 23–28 Ma and 34–36 Ma from the core of the klippe and suggested an older thermal event in the Kathmandu klippe. A sample from a Cambro-Ordovician granite, the Palung granite, in the southern part of the Kathmandu klippe yields an $^{40}Ar/^{39}Ar$ age of 18–24 Ma [*Arita et al*., 1997], comparable with a ~20 Ma $^{40}Ar/^{39}Ar$ muscovite age [*Bollinger et al*., 2004] from the southern limb of the Kathmandu klippe close to the MCT. Such early cooling of the Kathmandu klippe is consistent with its emplacement along a thrust active earlier and at higher structural levels than the MCT.

Kohn et al. [2004] first proposed an intra-GHS thrust (the Langtang thrust) ~10 km north of the MCT based on monazite geochronology and inferred an old activation age of ~21 ± 2 Ma based on in situ $^{208}Pb/^{232}Th$ dating of chemically distinct monazite domains [see also *Kohn et al*., 2005]. Since then, several other intra-GHS thrusts have also been proposed. These include the Toijem shear zone in western Nepal, active between 17 and 26 Ma [*Carosi et al*., 2007, 2010]; the Mangri shear zone in western Nepal, initiating ~25 Ma [*Montomoli et al*., 2013]; the Bhanuwa and Sinuwa thrusts in central Nepal, active 19–27 Ma [*Corrie and Kohn*, 2011]; and the Higher Himalayan thrust in eastern Nepal, active 22–27 Ma [*Goscombe et al*., 2006; *Imayama et al*., 2012]. The along-strike continuity of these thrusts is not known, but collectively, they imply that the GHS was not all emplaced along one thrust. The spatial and temporal variations of such faults in the GHS must be determined to understand the evolution of the Himalayan thrust belt. Although we cannot yet definitively link the Galchhi shear zone to a specific intra-GHS thrust, chronologic disparity relative to the MCT recommends correlation to one of them.

A depositional contact between the GHS and THS in the Kathmandu klippe [*Stöcklin*, 1980; *Gehrels et al*., 2006] implies that when the basal thrust to the Kathmandu klippe was active, THS rocks must have been passively carried on the hanging wall(s). Recognizing that there are three shear zones in the immediate Galchhi area (from lowest to highest the RMT, MCT, and Galchhi shear zone) and that the Galchhi shear zone likely juxtaposes high-grade GHS, we propose correlating the Galchhi shear zone with the next-highest intra-GHS thrust in the region—the Langtang thrust. Both thrusts carry GHS in hanging wall and footwall, and ages of inferred movement overlap within uncertainty. Alternatively, the Galchhi shear zone could correlate with an older intra-GHS thrust, such as the Sinuwa or Bhanuwa thrusts [*Corrie and Kohn*, 2011].

9. Kinematic Model

The older age of 20–29 Ma for Galchhi shear zone movement predates slip on the MCT and does not fit into previous 2-thrust (intra-LHS), 1-thrust (= MCT), or passive roof thrust models for the evolution of the Kathmandu klippe. Here we present a viable kinematic model that incorporates the older thrusting event from Galchhi in the context of the potential link with the intra-GHS Langtang thrust. Alternate assumptions that the Galchhi shear zone correlates with a different intra-GHS thrust do not affect our conclusions. In Figure 12, the length and thickness of each thrust sheet is from *Pearson* [2002], *Khanal and Robinson* [2013], and field measurements of the location of the thrust sheets. We estimate minimum length of thrust sheets as the minimum amount needed to cover the thrust sheet in the footwall.

The model begins with an assumed simple configuration of the Indian passive margin sequence (Figure 12a) and initiation of motion on the Langtang thrust at ~22 Ma (Figure 12b) that carried GHS and THS in its hanging wall with a slip magnitude of ~160 km. The Langtang thrust cut upward stratigraphically through GHS in a southward tapering ramp so that the hanging wall sheet formed a long wedge shape (Figures 12a and 12b). We do not assume the entire GHS had a constant thickness, and it may instead have thinned southward. The Langtang thrust sheet completely covered the future MCT sheet and almost half of the future RMT sheet (Figure 12b). As the hinterland thickened with the emplacement of the Langtang thrust sheet, the STDS system activated around 19–22 Ma in central Nepal [*Searle and Godin*, 2003; *Sachan et al*., 2010], possibly because the topography was unable to support the wedge. Alternatively, the STDS could have been active briefly between 23 and 25 Ma [*Carosi et al*., 2013], prior to motion on the Langtang thrust. Motion on the MCT sheet spanned 16–10 Ma [*Kohn et al*., 2004; *Montomoli et al*., 2013] and passively carried the Langtang thrust sheet and overlying THS sheet (Figure 12c). Minimum slip on the MCT in central Nepal was ~75 km, which is considerably less than the hundreds of kilometers proposed in other locations [*DeCelles et al*., 2001; *Robinson et al*., 2006; *Khanal and Robinson*, 2013]; however, the discrepancy is explained by the ~160 km of slip

along the Langtang thrust. After the MCT was emplaced, slip was transferred southward at 10 Ma to the RMT [*Kohn et al*., 2004; *Kohn*, 2008], which passively transported the overlying MCT sheet, Langtang thrust sheet and THS (Figure 12d).

The Lesser Himalayan duplex system activated at ~7–3 Ma [*Kohn*, 2008], first with motion on the Trishuli thrust, followed by emplacement of the Lesser Himalayan thrust sheets [*Khanal and Robinson*, 2013] (Figure 12e). Younger $^{40}Ar/^{39}Ar$ ages (10–5 Ma) near the MCT [*Arita et al*., 1997; *Harrison et al*., 1998; *Macfarlane et al*., 1992] and zircon and apatite fission track ages (<3 Ma) [*Arita and Ganzawa*, 1997; *Robert et al*., 2011] are interpreted to reflect the building of the Lesser Himalayan duplex system. Emplacement of the LHD system folded overlying thrust sheets into a broad anticlinorium (e.g., the Gorkha-Pokhara antiform) and tilted the northern part of the Kathmandu klippe southward (Figure12f). This explains why rocks dip southward at Galchhi [*Johnson et al*., 2001].

The Main Boundary thrust cuts the upper Siwalik unit in central Nepal [*Khanal and Robinson*, 2013], which ranges in age from ~4.1 to 2.5 Ma [*Rösler et al*., 1997; *Ojha et al*., 2008]; thus, the Main Boundary thrust might have initiated ~3 Ma or later in central Nepal. The MBT folded the leading edge of the thrust sheet and overlying Kathmandu klippe to dip to the north in the southern part of the Kathmandu klippe (Figure 12f). Finally, the MFT, active since mid-Pliocene time [*Lavé and Avouac*, 2000; *Sapkota et al*., 2012], transported Subhimalayan rocks on top of the undeformed Subhimalayan rocks and Indo-Gangetic plain (Figure 12g), which increased the northward dip of the southern limb of the Kathmandu klippe.

This model does not explain top-to-the-north shear fabrics [*Webb et al*., 2011a] that are superimposed on the broad age and metamorphic patterns on which our interpretations are based. Penetrative, postthickening extension has been documented at a similar structural level in central Bhutan [*Long and McQuarrie*, 2010; *Corrie et al*., 2012] and ascribed to wedge collapse in the context of metamorphically driven changes to wedge rheology and/or structurally driven changes to boundary conditions. A similar process might explain both extensional shear fabrics and the inconsistency of shear direction at Galchhi.

Garnet porphyroblasts close to the Galchhi shear zone contain inclusion trails that preserve a pre-MCT tectonometamorphic history [*Sapkota and Sanislav*, 2013] and record average P-T conditions of ~11.5 kbar and ~680°C [*Johnson et al*., 2001; *Sapkota and Sanislav*, 2013], broadly consistent with P-T conditions of kyanite gneiss in the Langtang region [*Kohn*, 2008] in the footwall of the Langtang thrust. At Galchhi, P-T estimates imply a ~150°C decrease northward toward the MCT over a structural distance of ~1.5 km. If the Langtang thrust cut up section in the GHS at a relatively low angle (10–12°), rocks farther south in the thrust sheet should be stratigraphically higher (younger), and somewhat lower metamorphic grade. This configuration (Figure 12a) explains the lower temperature at Galchhi compared to Langtang, the permissively younger depositional ages (although age brackets overlap: ≤570 at Galchhi verus ≤660 at Langtang), and the decrease in thickness of the Kathmandu klippe rock toward the south compared to the north.

10. Tectonic Implications

Two end-member kinematic models of tectonic evolution of the Himalaya are currently debated. The channel flow model assumes that focused erosion on the frontal part of the thrust belt catalyzed ductile flow of middle crust toward the foreland driven by a lateral pressure gradient between Tibet and India [*Beaumont et al*., 2001, 2004; *Jamieson et al*., 2004]. In contrast, the critical taper model advocates southward propagation of the thrust belt, maintaining a critically tapered wedge [*Davis et al*., 1983; *Dahlen and Suppe*, 1984], by progressive underplating and duplex formation [*DeCelles et al*., 2001; *Robinson et al*., 2003, 2006; *Bollinger et al*., 2004, 2006; *Robinson*, 2008; *Kohn*, 2008; *Herman et al*., 2010; *Khanal and Robinson*, 2013]. Recent research asserts that both tectonic styles can coexist in large hot orogenic system [*Larson et al*., 2011; *Mukherjee*, 2013; *Jamieson and Beaumont*, 2013], but the relative contributions of each to overall architecture remain debated. Our observations indicate that the region is dominated by top-to-the-south shear. In this locality, the Lesser Himalayan duplex and Main Boundary thrust fold the Kathmandu klippe into a synclinorium with the hanging wall rock of the Galchhi shear zone almost vertical and progressively shallower dip toward south (Figure 3). Thus, the formation of the synclinorium and preservation of the Kathmandu klippe reflect late-stage wedge growth.

More generally, a growing geochronological data set suggests protracted propagation of the Himalayan thrust belt southward since 25–30 Ma, with accretion of progressively younger and lower metamorphic grade thrust sheets to the base of the wedge [e.g., see *Kohn et al*., 2004; *Kohn*, 2008, 2014]. Older movement on the Galchhi shear zone at 20–29 Ma overlaps the 16–27 Ma age of intra-GHS thrust sheet(s) [*Kohn et al*., 2004; *Goscombe et al*., 2006; *Carosi et al*., 2007, 2010; *Corrie and Kohn*, 2011; *Imayama et al*., 2012; *Montomoli et al*., 2013]. Thus, the Galchhi shear zone represents an older thrust emplaced prior to slip on the MCT and supports the hypothesis that the Himalaya developed through repeated transfer of Indian plate rocks as discrete sheets or rock to the hanging wall of the Main Himalayan thrust [*Kohn et al*., 2004; *Kohn*, 2008, 2014]. This is most consistent with the critical taper model proposed for the evolution of the Himalaya.

Slip on the STDS was restricted to a brief pulse between 19 and 22 Ma [*Hodges et al*., 1996; *Searle and Godin*, 2003; *Sachan et al*., 2010], or perhaps even earlier (23–25 Ma) [*Carosi et al*., 2013], long before motion on the MCT (16–10 Ma in the Langtang area) [*Kohn et al*., 2004; *Kohn*, 2008]. The vast simplification of protracted and synchronous motion on the MCT and STDS with opposite shear senses [*Beaumont et al*., 2001] does not hold true in central Nepal. Extension in the Galchhi area is restricted to late-stage minor normal brittle faults in the Galchhi shear zone that crosscut older deformed rocks (Figure 4b) [*Sapkota and Sanislav*, 2013], and east-west shear motion (Figure 4d) that possibly developed by sliding the steep southern limb of the broad anticlinorium with the growth of the Lesser Himalayan duplex system. Other klippen along the Himalaya that were emplaced on top of the Lesser Himalayan rock may have originated similarly along pre-MCT, intra-GHS thrusts. However, further research is needed to evaluate the geochronological evolution of the klippen to determine the orogen-wide implications of their emplacement along thrusts that predate the MCT.

11. Conclusions

Field, structural, and U-Pb geochronology from the Langtang and the Galchhi areas in central Nepal allow a reinterpretation of the origin of the Kathmandu klippe and permit critical assessment of the Himalayan tectonic models. The basal shear zone to the Kathmandu klippe (the Galchhi shear zone) was active sometime between 20 and 29 Ma, predating slip on the MCT by as much as 10 Ma or more. Rocks in the hanging wall and footwall of the Galchhi shear zone are at most Neoproterozoic in age so do not include lower LHS rocks. Thus, the Kathmandu klippe was most plausibly emplaced along an older, intra-GHS thrust, such as the Langtang thrust, not the MCT. Similar generations of top-to-the-south and top-to-the-north shear sense indicators do not uniquely support the passive roof thrust model, which correlates the Galchhi shear zone with the South Tibetan Detachment System. Diachroneity between slip on the Galchhi shear zone and MCT further argue against the passive roof thrust model.

The intra-Greater Himalayan thrust model proposed here implies that the Kathmandu klippe is the leading edge of the Langtang thrust sheet or an older and structurally higher thrust in the Greater Himalayan thrust system. These data imply that the Langtang thrust sheet and the Galchhi thrust sheet were continuous, that the Main Central Thrust sheet at both Langtang and Galchhi were also once continuous and that both continuous thrust sheets were erosionally breached during formation of the Lesser Himalayan duplex. These observations support the hypothesis that the Greater Himalayan Sequence in Nepal was not emplaced as a single body of rock but consists of two or more ductile thrust sheets. Underplating of Greater Himalayan thrust sheets accompanied progressive southward propagation of the thrust belt, which ultimately incorporated Lesser Himalayan and then Subhimalayan rocks.

Acknowledgments

Support for this project was provided to S. Khanal by a Geological Society of America Graduate Research Grant and sources at the University of Alabama, including the Geological Sciences Advisory Board (GSAB) Scholarship, Hooks Fund, Graduate School, Capstone International, and Graduate Student Services. We thank Saroj Khanal and Pramod Simkhada for providing field assistance; Bishal Nath Upreti and Kamal Kant Acharya for sharing their knowledge and experience of the Himalaya; and Harold Stowell, Andrew Goodliffe, and Ryan Ewing for providing fruitful suggestions. We thank the Arizona Laserchron Facility (NSF EAR 1032156). We thank Rodolfo Carosi, Sean Long, and Associate Editor Lindsay Schoenbohm, for their constructive reviews. This work was supported by NSF grants EAR 1048124 and EAR 1321897 to M.J.K. and EAR 0809405 to D.M.R. All analytical data are in Table S1 in the supporting information.

References

Acharya, K. K. (2008), Qualitative, Kinematic investigations related to the extrusion of the Higher Himalayan crystalline and equivalent tectonometamorphic wedges in central Nepal Himalaya, PhD dissertation, Univ. of Vienna, Austria.

Arita, K., and Y. Ganzawa (1997), Thrust tectonics and uplift process of the Nepal Himalaya revealed from fission-track ages, *J. Geogr.-Tokyo*, *106*, 156–167.

Arita, K., R. D. Dallmeyer, and A. Takasu (1997), Tectonothermal evolution of the Lesser Himalaya, Nepal: Constraints from 40Ar/39Ar ages from the Kathmandu Nappe, *Island Arc.*, *6*(4), 372–385.

Avouac, J. P. (2003), Mountain building, erosion, and the seismic cycle in the Nepal Himalaya, *Adv. Geophys.*, *46*, 1–80, doi:10.1016/S0065-2687(03)46001-9.

Beaumont, C., R. A. Jamieson, M. H. Nguyen, and B. Lee (2001), Himalayan tectonics explained by extrusion of a low viscosity channel coupled to focused surface denudation, *Nature*, *414*, 738–742, doi:10.1038/414738a.

Beaumont, C., R. A. Jamieson, M. H. Nguyen, and S. Medvedev (2004), Crustal channel flows: 1. Numerical models with applications to the tectonics of the Himalayan-Tibetan orogeny, *J. Geophys. Res.*, *109*, B06406, doi:10.1029/2003JB002809.
Bhattacharyya, K., and G. Mitra (2009), A new kinematic evolutionary model for the growth of a duplex-an example from the Rangit duplex, Sikkim Himalaya, India, *Gondwana Res.*, *16*, 697–715.
Bollinger, L., J. P. Avouac, O. Beyssac, E. J. Catlos, T. M. Harrison, M. Grove, and S. Sapkota (2004), Thermal structure and exhumation history of the Lesser Himalaya in central Nepal, *Tectonics*, *23*, TC5015, doi:10.1029/2003TC001564.
Bollinger, L., P. Henry, and J. P. Avouac (2006), Mountain building in the Nepal Himalaya: Thermal and kinematic model, *Earth Planet. Sci. Lett.*, *244*, 58–71, doi:10.1016/j.epsl.2006.01.045.
Brookfield, M. E. (1993), The Himalayan passive margin from Precambrian to Cretaceous times, *Sed. Geol.*, *84*(1), 1–35.
Burchfiel, B. C., Z. Chen, K. V. Hodges, Y. Liu, L. H. Royden, C. Deng, and J. Xu (1992), The South Tibetan detachment system, Himalayan orogen: Extension contemporaneous with and parallel to shortening in a collisional mountain belt, *Geol. Soc. Am. Spec. Pap.*, *269*, p. 41.
Caby, R., A. Pêcher, and P. Le Fort (1983), Le grand chevauchement central Himalayen: Nouvelles données sur le métamorphisme inverse à la base de la Dalle du Tibet, *Rev. Geol. Dyn. Géogr. Phys.*, *24*, 89–100.
Carosi, R., B. Lombardo, G. Molli, G. Musumeci, and P. C. Pertusati (1998), The South Tibetan detachment system in the Rongbuk valley, Everest region. Deformation features and geological implications, *J. Asian Earth Sci.*, *16*(2), 299–311.
Carosi, R., C. Montomoli, and D. Visonà (2007), A structural transect in the Lower Dolpo: Insights on the tectonic evolution of Western Nepal, *J. Asian Earth Sci.*, *29*(2), 407–423.
Carosi, R., C. Montomoli, D. Rubatto, and D. Visonà (2010), Late Oligocene high-temperature shear zones in the core of the Higher Himalayan Crystallines (Lower Dolpo, western Nepal), *Tectonics*, *29*, TC4029, doi:10.1029/2008TC002400.
Carosi, R., C. Montomoli, D. Rubatto, and D. Visonà (2013), Leucogranite intruding the South Tibetan detachment in western Nepal: Implications for exhumation models in the Himalayas, *Terra Nova*, *25*, 478–489, doi:10.1111/ter.12062.
Catlos, E. J., T. M. Harrison, M. J. Kohn, M. Grove, F. J. Ryerson, C. E. Manning, and B. N. Upreti (2001), Geochronologic and thermobarometric constraints on the evolution of the Main Central Thrust, central Nepal Himalaya, *J. Geophys. Res.*, *106*, 16,177–16,204, doi:10.1029/2000JB900375.
Cawood, P. A., M. R. Johnson, and A. A. Nemchin (2007), Early Palaeozoic orogenesis along the Indian margin of Gondwana: Tectonic response to Gondwana assembly, *Earth Planet. Sci. Lett.*, *255*(1), 70–84.
Colchen, M., P. Le Fort, and A. Pêcher (1986), Recherches géologiques dans l'Himalaya du Népal; Annapurna-Manaslu-Ganesh Himal. Editions du Centre National de la Recherche Scientifique., scale 1:200,000.
Coleman, M. E. (1996), Orogen-parallel and orogen-perpendicular extension in the central Nepalese Himalayas, *Geol. Soc. Am. Bull.*, *108*, 1594–1607.
Coleman, M. E. (1998), U-Pb constraints on Oligocene-Miocene deformation and anatexis within the central Himalaya, Marsyandi valley, Nepal, *Am. J. Sci.*, *298*(7), 553–571.
Copley, A., J. P. Avouac, and J. Y. Royer (2010), India-Asia collision and the Cenozoic slowdown of the Indian plate: Implications for the forces driving plate motions, *J. Geophys. Res.*, *115*, B03410, doi:10.1029/2009JB006634.
Corrie, S. L., and M. J. Kohn (2011), Metamorphic history of the central Himalaya, Annapurna region, Nepal, and implications for tectonic models, *Geol. Soc. Am. Bull.*, *123*(9–10), 1863–1879.
Corrie, S. L., M. J. Kohn, N. McQuarrie, and S. P. Long (2012), Flattening the Bhutan Himalaya, *Earth Planet. Sci. Lett.*, *349*, 67–74.
Dahlen, F. A., and J. Suppe (1984), Mechanics of fold-and-thrust belts and accretionary wedges: Cohesive coulomb theory, *J. Geophys. Res.*, *89*, 10,087–10,101.
Davis, D., J. Suppe, and F. A. Dahlen (1983), Mechanics of fold-and-thrust belts and accretionary wedges, *J. Geophys. Res.*, *88*, 1153–1172.
DeCelles, P. G., G. E. Gehrels, J. Quade, B. LaReau, and M. Spurlin (2000), Tectonic implications of U-Pb zircon ages of the Himalayan orogenic belt in Nepal, *Science*, *288*(5465), 497–499.
DeCelles, P. G., D. M. Robinson, J. Quade, T. P. Ojha, C. N. Garzione, P. Copeland, and B. N. Upreti (2001), Stratigraphy, structure, and tectonic evolution of the Himalayan fold-thrust belt in western Nepal, *Tectonics*, *20*, 487–509.
DeCelles, P. G., G. E. Gehrels, Y. Najman, A. J. Martin, A. Carter, and E. Garzanti (2004), Detrital geochronology and geochemistry of Cretaceous–Early Miocene strata of Nepal: Implications for timing and diachroneity of initial Himalayan orogenesis, *Earth Planet. Sci. Lett.*, *227*(3), 313–330.
Fraser, G., B. Worley, and M. Sandiford (2000), High-precision geothermobarometry across the High Himalayan metamorphic sequence, Langtang Valley, Nepal, *J. Metamorph. Geol.*, *18*, 665–681, doi:10.1046/j.1525-1314.2000.00283.x.
Gansser, A. (1964), *Geology of the Himalayas*, Wiley-Interscience, London.
Gautam, P., and W. Roesler (1999), Depositional chronology and fabric of Siwalik Group sediments in central Nepal from magnetostratigraphy and magnetic anisotropy, *J. Asian Earth Sci.*, *17*(5–6), 659–682.
Gehrels, G., et al. (2011), Detrital zircon geochronology of pre-Tertiary strata in the Tibetan-Himalayan orogeny, *Tectonics*, *30*, TC5016, doi:10.1029/2011TC002868.
Gehrels, G. E., P. G. DeCelles, A. Martin, T. P. Ojha, G. Pinhassi, and B. N. Upreti (2003), Initiation of the Himalayan orogen as an Early Paleozoic thin-skinned thrust belt, *GSA Today*, *18*(9), 4–9.
Gehrels, G. E., P. G. DeCelles, T. P. Ojha, and B. N. Upreti (2006), Geologic and U-Th-Pb geochronologic evidence for early Paleozoic tectonism in the Kathmandu thrust sheet, central Nepal Himalaya, *Geol. Soc. Am. Bull.*, *118*, 185–198, doi:10.1180/B25753.1.
Godin, L., R. R. Parrish, R. L. Brown, and K. V. Hodges (2001), Crustal thickening leading to exhumation of the Himalayan metamorphic core of central Nepal: Insight from U-Pb geochronology and $^{40}Ar/^{39}Ar$ thermochronology, *Tectonics*, *20*, 729–747, doi:10.1029/2000TC001204.
Goscombe, B., D. Gray, and M. Hand (2006), Crustal architecture of the Himalayan metamorphic front in eastern Nepal, *Gondwana Res.*, *10*(3), 232–255.
Grujic, D. (2006), Channel flow and continental collision tectonics: An overview, in *Channel Flow, Extrusion and Exhumation in Continental Collision Zones*, edited by R. D. Law and M. P. Searle, *Geol. Soc. London Spec. Publ.*, *268*, 25–37, doi:10.1144/GSL.SP.2006.268.01.02.
Guillot, S. (1999), An overview of the metamorphic evolution in central Nepal, *J. Asian Earth Sci.*, *17*(5–6), 718–725.
Harrison, T. M., P. Copeland, W. S. F. Kidd, and A. Yin (1992), Raising Tibet, *Science*, *255*, 1663–1670.
Harrison, T. M., K. D. McKeegan, and P. Le Fort (1995), Detection of inherited monazite in the Manaslu leucogranite by $^{208}Pb/^{232}Th$ ion microprobe dating: Crystallization age and tectonic significance, *Earth Planet. Sci. Lett.*, *183*, 271–282.
Harrison, T. M., O. M. Lovera, and M. Grove (1997), New insights into the origin of two contrasting Himalayan granite belts, *Geology*, *25*(10), 899–902.
Harrison, T. M., M. Grove, O. M. Lovera, and E. J. Catlos (1998), A model for the origin of Himalayan anatexis and inverted metamorphism, *J. Geophys. Res.*, *103*, 27,017–27,032.

Harrison, T. M., E. J. Catlos, and J. M. Montel (2002), U-Th-Pb dating of phosphate minerals, in *Phosphates: Geochemical, Geobiological and Materials Importance*, edited by J. M. Hughes, M. Kohn, and J. Rakovan, pp. 523–528, Mineralogical Soc. Am., Washington, D. C.
Heim, A., and A. Gansser (1939), Central Himalaya: Geological observations of the Swiss expedition, *Mem. Soc. Helv. Sci. Nat.*, *73*, 1–245.
Herman, F., et al. (2010), Exhumation, crustal deformation, and thermal structure of the Nepal Himalaya derived from the inversion of thermochronological and thermobarometric data and modeling of the topography, *J. Geophys. Res.*, *115*, B06407, doi:10.1029/2008JB006126.
Hodges, K. V. (2000), Tectonics of the Himalaya and southern Tibet from two perspectives, *Geol. Soc. Am. Bull.*, *112*(3), 324–350.
Hodges, K. V., R. R. Parrish, and M. P. Searle (1996), Tectonic evolution of the central Annapurna Range, Nepalese Himalayas, *Tectonics, 15*, 1264–1291.
Hubbard, M. S., and T. M. Harrison (1989), 40Ar/39Ar age constraints on deformation and metamorphism in the Main Central Thrust zone and Tibetan Slab, eastern Nepal Himalaya, *Tectonics*, *8*, 865–880.
Huntington, K. W., A. E. Blythe, and K. V. Hodges (2006), Climate change and Late Pliocene acceleration of erosion in the Himalaya, *Earth Planet. Sci. Lett.*, *252*(1), 107–118.
Iaccarino, S., C. Rodolfo, C. Montomoli, A. Langone, and D. Visonà (2012), Structural, metamorphic and geochronologic constrains of a ductile shear zone within the core of Higher Himalayan Crystallines in western Nepal: The Mangri Shear Zone, in *The 27th Himalaya-Karakoram-Tibet Workshop (HKT)*, *Bull. Nepal Geol. Soc.*, *134*, 158.
Iaccarino, S., C. Montomoli, R. Carosi, and A. Langone (2013), Linking microstructures, petrology and in situ U-(Th)-Pb geochronology to constrain PTtD evolution of the Greather Himalayan Sequences in Western Nepal (Central Himalaya), in *EGU General Assembly Conference Abstracts*, *15*, 2342.
Imayama, T., et al. (2012), Two-stage partial melting and contrasting cooling history within the Higher Himalayan Crystalline Sequence in the far-eastern Nepal Himalaya, *Lithos, 134*, 1–22.
Inger, S., and N. B. W. Harris (1992), Tectonothermal evolution of the High Himalayan crystalline sequence, Langtang Valley, northern Nepal, *J. Metamorph. Geol.*, *10*(3), 439–452.
Jamieson, R. A., and C. Beaumont (2013), On the origin of orogens, *Geol. Soc. Am. Bull.*, *125*, 1671–1702, doi:10.1130/B30855.1.
Jamieson, R. A., C. Beaumont, M. H. Nguyen, and B. Lee (2002), Interaction of metamorphism, deformation, and exhumation in large convergent orogens, *J. Metamorph. Geol.*, *20*, 1–16.
Jamieson, R. A., C. Beaumont, S. Medvedev, and M. H. Nguyen (2004), Crustal channel flows: 2. Numerical models with implications for metamorphism in the Himalayan-Tibetan orogeny, *J. Geophys. Res.*, *109*, B06407, doi:10.1029/2003JB002811.
Johnson, M. R. W., and G. Rogers (1997), Rb-Sr ages of micas from the Kathmandu complex, Central Nepalese Himalaya: Implications for the evolution of the Main Central Thrust, *Geol. Soc. Am. Bull.*, *154*(5), 863–869.
Johnson, M. R. W., G. J. H. Oliver, R. R. Parrish, and S. P. Johnson (2001), Synthrusting metamorphism, cooling, and erosion of the Himalayan Kathmandu Complex, Nepal, *Tectonics*, *20*, 394–415.
Khanal, S., and D. M. Robinson (2012a), Evidence of two parallel, orogen scale thrust sheets bounding the base of the Greater Himalaya in Central Nepal, Geol. Soc. Am Abstr. with Prog., 44.
Khanal, S., and D. M. Robinson (2012b), Is the fault that carries the Kathmandu klippe the Main Central Thrust or an intra-Greater Himalayan thrust?, in *The 27th Himalaya-Karakoram-Tibet Workshop (HKT)*, *J. Nepal Geol. Soc.*, *45*, 176.
Khanal, S., and D. M. Robinson (2013), Upper crustal shortening and forward modeling of the Himalayan thrust belt along the Budhi-Gandaki River, central Nepal, *Int. J. Earth Sci.*, *102*, 1871–1891, doi:10.1007/s00531-013-0889-1.
Khanal, S., D. M. Robinson, S. Mandal, and P. Simkhada (2014), Structural, geochronological and geochemical evidence for two distinct thrust sheets in the "Main Central Thrust zone," the Main Central Thrust and Ramgarh-Munsiari thrust: Implications for upper crustal shortening in central Nepal, in *Tectonics of the Himalaya*, *Geol. Soc. Spec. Publ.*, edited by S. Mukherjee et al., p. 412, doi:10.1144/SP412.2.
Kohn, M. J. (2008), P-T-t data from central Nepal support critical taper and repudiate large scale channel flow of the Greater Himalayan Sequence, *Geol. Soc. Am. Bull.*, *120*, 259–273, doi:10.1130/B26252.1.
Kohn, M. J. (2014), Himalayan metamorphism and its tectonic implications, *Ann. Rev. Earth Planet Sci.*, *42*, 381–419, doi:10.1146/annurev-earth-060313-055005.
Kohn, M. J., M. Wieland, C. D. Parkinson, and B. N. Upreti (2004), Miocene faulting at plate tectonic velocity in the Himalaya of central Nepal, *Earth Planet. Sci. Lett.*, *228*, 299–310, doi:10.1016/j.epsl.2004.10.007.
Kohn, M. J., M. S. Weiland, C. D. Parkinson, and B. N. Upreti (2005), Five generations of monazite in Langtang gneisses: Implications for chronology of the Himalayan metamorphic core, *J. Meta. Petrol.*, *23*, 399–406, doi:10.1111/j.1525-1314.2005.00584.x.
Kohn, M. J., S. K. Paul, and S. L. Corrie (2010), The lower Lesser Himalayan sequence: A Paleoproterozoic arc on the northern margin of the Indian plate, *Geol. Soc. Am. Bull.*, *122*, 323–335.
Larson, K. P., J. M. Cottle, and L. Godin (2011), Petro chronologic record of metamorphism and melting in the upper Greater Himalayan sequence, Manaslu–Himal Chuli Himalaya, west-central Nepal, *Lithosphere*, *3*, 379–392, doi:10.1130/L149.1.
Lavé, J., and J. P. Avouac (2000), Active folding of fluvial terraces across the Siwaliks Hills, Himalayas of central Nepal, *J. Geophys. Res.*, *105*, 5735–5770.
Le Fort, P. (1975), Himalayas: The collided range, Present knowledge of the continental arc, *Am. J. Sci.*, *275*(A), 1–44.
Le Fort, P., F. Debon, A. Pêcher, and J. V. P. Sonet (1986), The 500 Ma magmatic event in alpine southern Asia, a thermal episode at Gondwana scale, in *Évolution des Domaines Orogéniques d'Asie Méridionale (de la Turquie à l'Indonésie)*, edited by P. Le Fort, M. Colchen, and C. Montenat, pp. 191–209, Science de la Terre, Nancy, France.
Long, S., and N. McQuarrie (2010), Placing limits on channel flow: Insights from the Bhutan Himalaya, *Earth Planet. Sci. Lett.*, doi:10.1016/j.epsl.2009.12.033.
Ludwig, K. R. (2008), *Manual for Isoplot 3.7, Spec. Publ. 4*, 77 pp., Berkeley Geochronology Center, Berkeley, Calif.
Lyon-Caen, H., and P. Molnar (1985), Gravity anomalies, flexure of the Indian plate, and the structure, support and evolution of the Himalaya and Ganga Basin, *Tectonics*, *4*, 518–538.
Macfarlane, A. M. (1993), Chronology of tectonic events in the crystalline core of the Himalaya, Langtang National Park, central Nepal, *Tectonics*, *12*, 1004–1025.
Macfarlane, A. M. (1995), An evaluation of the inverted metamorphic gradient at Langtang National Park, central Nepal Himalaya, *J. Metamorph. Geol.*, *13*(5), 595–612.
Macfarlane, A. M., K. V. Hodges, and D. Lux (1992), A structural analysis of the Main Central Thrust zone, Langtang National Park, central Nepal Himalaya, *Geol. Soc. Am. Bull.*, *104*(11), 1889–1402.
Martin, A. J., P. G. DeCelles, G. E. Gehrels, P. J. Patchett, and C. Isachsen (2005), Isotopic and structural constraints on the location of the Main Central Thrust in the Annapurna Range, central Nepal Himalaya, *Geol. Soc. Am. Bull.*, *117*(7-8), 926–944, doi:10.1130/B25646.1.

Martin, A. J., J. Ganguly, and P. G. DeCelles (2010), Metamorphism of Greater and Lesser Himalayan rocks exposed in the Modi Khola valley, central Nepal, *Contrib. Mineral. Petrol.*, *159*, 203–223, doi:10.1007/s00410-009-0424-3.

Montomoli, C., S. Iaccarino, R. Carosi, A. Langone, and D. Visonà (2013), Tectonometamorphic discontinuities within the Greater Himalayan Sequence in Western Nepal (Central Himalaya): Insights on the exhumation of crystalline rocks, *Tectonophysics*, doi:10.1016/j.tecto.2013.06.006.

Mukherjee, S. (2013), Higher Himalayan Shear Zone, Bhagirathi section (NW Himalaya, India)—Its structures, back thrusts, and extrusion mechanism by both channel flow and critical taper mechanisms, *Int. J. Earth Sci.*, doi:10.1007/s00531-012-0861-5.

Myrow, P. M., N. C. Hughes, T. S. Paulsen, I. S. Williams, S. K. Parcha, K. R. Thompson, S. A. Bowring, A. C. Peng, and A. D. Ahluwalia (2003), Integrated tectonostratigraphic analysis of the Himalaya and implications for its tectonic reconstruction, *Earth Planet. Sci. Lett.*, *212*(3), 433–441.

Myrow, P. M., N. C. Hughes, M. P. Searle, C. M. Fanning, S. C. Peng, and S. K. Parcha (2009), Stratigraphic correlation of Cambrian-Ordovician deposits along the Himalaya: Implications for the age and nature of rocks in the Mount Everest region, *Geol. Soc. Am. Bull.*, *121*(3–4), 323–332.

Najman, Y., et al. (2010), Timing of India–Asia collision: Geological, biostratigraphic, and palaeomagnetic constraints, *J. Geophys. Res.*, *115*, B12416, doi:10.1029/2010JB007673.

Ojha, T. P., R. F. Butler, J. Quade, P. G. DeCelles, D. Richards, and B. N. Upreti (2000), Magnetic polarity stratigraphy of the Neogene Siwalik Group at Khutia Khola, far western Nepal, *Geol. Soc. Am. Bull.*, *112*(3), 424–434.

Ojha, T. P., R. F. Butler, P. G. DeCelles, and J. Quade (2008), Magnetic polarity stratigraphy of the Neogene foreland basin deposits of Nepal, *Basin Res.*, doi:10.1111/j.1365-2117.2008.00374.x.

Pandey, M. R., R. P. Tandukar, J. P. Avouac, J. Lavé, and J. P. Massot (1995), Interseismic strain accumulation on the Himalayan crustal ramp (Nepal), *Geophys. Res. Lett.*, *22*, 751–754.

Parrish, R. R., and K. V. Hodges (1996), Isotopic constraints on the age and provenance of the Lesser and Greater Himalayan sequences, Nepalese Himalaya, *Geol. Soc. Am. Bull.*, *108*, 904–911.

Paudel, L. P., and K. Arita (2000), Tectonic and polymetamorphic history of the Lesser Himalaya in central Nepal, *J. Asian Earth Sci.*, *18*(5), 561–584.

Pearson, O. N. (2002), Structural evolution of the central Nepal fold-thrust belt and regional tectonic and structural significance of the Ramgarh thrust, PhD dissertation, Univ. of Ariz., Tucson.

Pearson, O. N., and P. G. DeCelles (2005), Structural geology and regional tectonic significance of the Ramgarh thrust, Himalayan fold-thrust belt of Nepal, *Tectonics*, *24*, TC4008, doi:10.1029/2003TC001617.

Pêcher, A. (1977), Geology of the Nepal Himalaya: Deformation and petrography in the Main Central Thrust zone, in *Himalaya: Sciences de la Terre*, edited by C. Jest, pp. 301–318, Centre National de la Recherche Scientifique, Paris.

Powell, C. M., and P. J. Conaghan (1973), Plate tectonics and the Himalayas, *Earth Planet. Sci. Lett.*, *20*, 1–20, doi:10.1016/0012-821X(73)90134-9.

Rai, S. M., S. Guillot, P. Le Fort, and B. N. Upreti (1998), Pressure-temperature evolution in the Kathmandu and Gosainkunda regions, central Nepal, *J. Asian Earth Sci.*, *16*, 283–298.

Ratschbacher, L., W. Frisch, and L. Guanghua (1994), Distributed deformation in southern and western Tibet during and after the India-Asia collision, *J. Geophys. Res.*, *99*, 19,917–19,945.

Robert, X., P. van der Beek, J. Braun, C. Perry, and J.-L. Mugnier (2011), Control of detachment geometry on lateral variations in exhumation rates in the Himalaya: Insights from low-temperature thermochronology and numerical modeling, *J. Geophys. Res.*, *116*, B05202, doi:10.1029/2010JB007893.

Robinson, D. M. (2008), Forward modeling the kinematic sequence of the central Himalayan thrust belt, western Nepal, *Geosphere*, *4*(5), 785–801, doi:10.1130/GES00163.1.

Robinson, D. M., and A. J. Martin (2014), Reconstructing the greater Indian margin: A balanced cross section in central Nepal focusing on the Lesser Himalayan duplex, *Tectonics*, doi:10.1002/2014TC003564.

Robinson, D. M., and O. N. Pearson (2013), Was Himalayan normal faulting triggered by initiation of the Ramgarh–Munsiari thrust and development of the Lesser Himalayan duplex?, *Int. J. Earth Sci.*, *102*, 1773–1790.

Robinson, D. M., P. G. DeCelles, C. N. Garzione, O. N. Pearson, T. M. Harrison, and E. J. Catlos (2003), Kinematic model for the Main Central Thrust in Nepal, *Geology*, *31*, 359–362, doi:10.1130/0091-7613(2003)031<0359:KMFTMC>2.0.CO;2.

Robinson, D. M., P. G. DeCelles, and P. Copeland (2006), Tectonic evolution of the Himalayan thrust belt in western Nepal: Implications for channel flow models, *Geol. Soc. Am. Bull.*, *118*, 865–885, doi:10.1130/B25911.1.

Rösler, W., W. Metzler, and E. Appel (1997), Neogene magnetic polarity stratigraphy of some fluviatile Siwalik sections, Nepal, *Geophys. J. Int.*, *130*(1), 89–111.

Rowley, D. B. (1996), Age of initiation of collision between India and Asia: A review of stratigraphic data, *Earth Planet. Sci. Lett.*, *145*(1), 1–13.

Rubatto, D. (2002), Zircon trace element geochemistry: Partitioning with garnet and the link between U-Pb ages and metamorphism, *Chemical Geol.*, *184*(1), 123–138.

Sachan, H. K., M. J. Kohn, A. Saxena, and S. L. Corrie (2010), The Malari leucogranite, Garhwal Himalaya, northern India: Chemistry, age, and tectonic implications, *Geol. Soc. Am. Bull.*, *122*(11–12), 1865–1876.

Sapkota, J., and I. V. Sanislav (2013), Preservation of deep Himalayan PT conditions that formed during multiple events in garnet cores: Mylonitization produces erroneous results for rims, *Tectonophysics*, *587*, 89–106, doi:10.1016/j.tecto.2012.10.029.

Sapkota, S. N., L. Bollinger, Y. Klinger, P. Tapponnier, Y. Gaudemer, and D. Tiwari (2012), Primary surface ruptures of the great Himalayan earthquakes in 1934 and 1255, *Nat. Geosci.*, *6*, doi:10.1038/NGEO1669.

Searle, M. P. (2010), Low-angle normal faults in the compressional Himalayan orogen: Evidence from the Annapurna–Dhaulagiri Himalaya, Nepal, *Geosphere*, *6*(4), 296–315.

Searle, M. P., and L. Godin (2003), The South Tibetan detachment and the Manaslu leucogranite: A structural reinterpretation and restoration of the Annapurna-Manaslu Himalaya, Nepal, *J. Geol.*, *111*, 505–523, doi:10.1086/376763.

Searle, M. P., R. D. Law, L. Godin, K. P. Larson, M. J. Streule, J. M. Cottle, and M. J. Jessup (2008), Defining the Himalayan Main Central Thrust in Nepal, *J. Geol. Soc.*, *165*(2), 523–534.

Stöcklin, J. (1980), Geology of Nepal and its regional frame, *J. Geol. Soc. London*, *187*, 1–34.

Thiede, R. C., B. Bookhagen, J. R. Arrowsmith, E. R. Sobel, and M. R. Strecker (2004), Climatic control on rapid exhumation along the Southern Himalayan Front, *Earth Planet. Sci. Lett.*, *222*(3), 791–806.

Thiede, R. C., J. R. Arrowsmith, B. Bookhagen, M. O. McWilliams, E. R. Sobel, and M. R. Strecker (2005), From tectonically to erosionally controlled development of the Himalayan orogeny, *Geology*, *33*(8), 689–692.

Upreti, B. N. (1999), An overview of the stratigraphy and tectonics of the Nepal Himalaya, *J. Asian Earth Sci.*, *17*(5–6), 577–606.

Upreti, B. N., and P. Le Fort (1999), Lesser Himalayan Crystalline Nappes of Nepal: Problem of their origin, in Advances on the geology of the Himalaya, focus on Nepal geology, *J. Asian Earth Sci.*, *328*, 225–238.

Watson, E. B., and T. M. Harrison (1983), Zircon saturation revisited: Temperature and composition effects in a variety of crustal magma types, *Earth Planet. Sci. Lett.*, *64*(2), 295–304.

Webb, A. A. G., A. K. Schmitt, D. He, and E. L. Weigand (2011a), Structural and geochronological evidence for the leading edge of the Greater Himalayan Crystalline complex in the central Nepal Himalaya, *Earth Planet. Sci. Lett.*, *304*(3), 483–495.

Webb, A. A. G., A. Yin, T. M. Harrison, J. Célérier, G. E. Gehrels, C. E. Manning, and M. Grove (2011b), Cenozoic tectonic history of the Himachal Himalaya (northwestern India) and its constraints on the formation mechanism of the Himalayan orogeny, *Geosphere*, *7*(4), 1013–1061.

Wobus, C. W., K. V. Hodges, and K. X. Whipple (2003), Has focused denudation sustained active thrusting at the Himalayan topographic front?, *Geology*, *31*(10), 861–864.

Wobus, C. W., K. X. Whipple, and K. V. Hodges (2006), Neotectonics of the central Nepalese Himalaya: Constraints from geomorphology, detrital 40Ar/39Ar thermochronology, and thermal modeling, *Tectonics*, *25*, TC4011, doi:10.1029/2005TC001935.

Yin, A. (2006), Cenozoic tectonic evolution of the Himalayan orogen as constrained by along-strike variation of structural geometry, exhumation history, and foreland sedimentation, *Earth Sci. Rev.*, *76*(1), 1–131.

Yin, A., and T. M. Harrison (2000), Geologic evolution of the Himalayan-Tibetan orogeny, *Ann. Rev. Earth Planet. Sci.*, *28*(1), 211–280.

Zhang, J., and L. Guo (2007), Structure and geochronology of the southern Xainza-Dinggye rift and its relationship to the south Tibetan detachment system, *J. Asian Earth Sci.*, *29*, 722–736.

Zhao, W., K. D. Nelson, and project INDEPTH Team (1993), Deep seismic-reflection evidence continental underthrusting beneath southern Tibet, *Nature*, *366*, 557–559.